



UNIVERSIDADE DA BEIRA INTERIOR
Engenharia

Sandwich Structures with Cork Agglomerate Cores for Thermal Insulation Purposes in Aircraft

Demis Rodrigues Peixoto

Dissertação para obtenção do Grau de Mestre em
Engenharia Aeronáutica
(Ciclo de estudos integrado)

Orientador: Prof. Doutor Francisco Miguel Ribeiro Proença Brojo
Coorientador: Prof. Doutor Pedro Vieira Gamboa

Covilhã, outubro de 2014

Acknowledgements

The author wishes to express his sincere gratitude to everyone who, in some form or way, contributed to the realization of the present thesis. Reaching this milestone would not have been possible if it were not for the support of several people who play an important part in my life.

To Dr. Francisco Brojo, my supervisor, for his constant availability and attention, for his valuable knowledge and advice, for always keeping me motivated through positive attitude and for his crucial support.

To Dr. Pedro Gamboa, my co-supervisor, for his inestimable input and for mentoring me in a variety of aspects throughout my investigation.

To Dr. José Miguel Silva, for introducing me to the DesAir Project, for encouraging me to take this challenge and also for his tireless dedication during the early stages of this work.

To Filipe Couceiro, for his readiness and availability whenever I needed assistance, for his knowledge and help in the numerical simulations as well as the experimental tests and for his presence and friendship in my life.

To Soraia Gomes, for her tireless support and comprehension throughout my academic life, for her invaluable input and advice in moments when I had to make the toughest decisions and finally for always being a pillar in my life. Thank you for walking this path with me. You will always have a special place in my heart. I love you.

To my parents, Maria do Céu Rodrigues and César Peixoto, my grandfather, Alberto Rodrigues and my grandmother, Arminda Pereira, for their unconditional love and support, for always believing in me in moments when I doubted my capabilities and for their sacrifice in order to grant me the chance to study and become a better person.

To Carlos Faustino, whose presence in my life plays a very big role in the success I have had, for his constant support and sacrifice and for being the person I needed the most when no one else could. You taught me to be a better man.

To Ryan Leslie, for giving me the inspiration to become the best person I can be which enabled me to overcome all the obstacles I found throughout my academic life and go beyond what everyone expected me to do.

To Amorim Cork Composites, for providing me with materials such as the cork agglomerate plates and the aluminum sheets.

Last but not least, to all my close friends and family that I did not mention here. Although I cannot put into words what you mean to me, I want you all to know that I cherish each and every one of you. Each person taught me something special that I will take with me in my journey of life. Thank you all.

Abstract

As the use of sandwich structures continues to increase rapidly for applications ranging from satellites, aircraft, ships, automobiles, rail cars, wind energy systems, and bridge construction (to mention only a few), lightweight and high strength structures have become indispensable to many high-tech industries such as aerospace, civil infrastructure and vehicle. Therefore, the demand for new materials has been rising which in turn led to the increasing use of composite sandwich structures applications. Utilizing natural materials over traditional synthetic structures allows avoiding the use of oil and other carbon products for the fabrication, which were otherwise needed, thus resulting in a reduction of carbon emissions. Besides being renewable, these materials provide such benefits as being both biodegradable and recyclable.

In its simplest form a structural sandwich is composed of two thin stiff face sheets and a thick lightweight core bonded between them. The properties of primary interest for the core materials can be summarized as: low density, high shear modulus, high shear strength, elevated stiffness perpendicular to the faces and both good thermal and acoustic insulation characteristics. The commonly used core materials are foams, balsa wood and honeycombs, the latter consisting in superlight structures with high strength-to-weight and stiffness-to-weight ratios. Honeycombs can be defined as an array of open cells, formed from sheets of suitable material, bonded together at controlled intervals and then expanded to form hexagonal cells. However, recent developments resulted into new alternatives like cellular core structures such as the case of cork. Cork has an alveolar cellular structure similar to that of a honeycomb, and its cells are mostly formed by suberin, lignin and cellulose. Although it seems that natural cork has a poor mechanical behavior when compared with other types of core materials, such as synthetic foams, for some specific applications, cork can actually compete with these materials. Its low thermal conductivity combined with a reasonable compressive strength makes it an excellent material for thermal insulation purposes as well as for applications in which compressive loads are present.

The work herein presented aims to study the feasibility of implementing cork, more specifically the NL20 cork agglomerate fabricated by Amorim Cork Composites, as the core material of sandwich structures with aluminum face sheets (Aalco 5754) by thermally characterizing nine circular sandwich panel samples through experimental tests. Taking into account the enormous challenges imposed by the global stake-holders of drastically reducing (75% per passenger/km) the environmental impact, such as the CO₂ emissions associated to the current manufacturing, as well as the operational and maintenance technologies of the various ways of transport, it becomes paramount that aeronautical industry starts incorporating a high amount of recyclable components, in addition to being lighter. Therefore, one of the key objectives of this study is to lower the weight of the samples whilst maintaining their thermal characteristics by drilling different hole patterns into their cork cores. The core configurations differ in hole shape,

diameter and depth so that their impact could be assessed. However, a uniform sample is included which served as the reference model for all others. The impact of the core's mass regarding the component's insulating ability was also investigated. All samples, which are thermally insulated on the sides in order to ensure one dimensional heat flow, were heated up to 80°C on the bottom face sheet and their individual insulating ability was determined by the measurement of the temperature at the center of the top face sheet with a contact thermocouple. The temperature distribution on the top face sheets was also recorded by a thermographic infrared camera positioned above the samples. The numerical analysis were carried out by resorting to the finite element code ABAQUS® v6.10-1. The experimental tests had to be performed first so that the experimental convective heat transfer coefficient could be determined and subsequently used in the numerical analysis. Heat transfer through radiation was proven to have very little influence on the results due to the small temperature differences between the samples and the surroundings, thus being practicably negligible.

The conclusions drawn from the comparison between the experimental and the numerical results allow taking an important step towards the adoption of cork as the material of choice for the core of sandwich structures and should serve as basis or reference for future more detailed studies in this area.

Keywords: Cork; Sandwich Structures; Thermal Characterization; Numerical Analysis; Insulating ability; Hole patterns

Resumo

À medida que o recurso a estruturas sandwich continua a aumentar rapidamente para aplicações que vão desde satélites, aeronaves, navios, automóveis, veículos ferroviários a sistemas de energia eólica e construção de pontes (mencionando apenas alguns), estruturas leves e com resistência elevada tornaram-se indispensáveis para muitas indústrias de alta tecnologia tais como a aeroespacial, civil e de transporte em geral. Sendo assim, a procura de novos materiais tem vindo a aumentar o que por sua vez levou ao aumento da utilização de aplicações de estruturas sandwich de compósitos. A utilização de materiais naturais no lugar de estruturas sintéticas tradicionais permite evitar o uso de óleos e outros produtos de carbono para a fabricação, que caso contrário seriam necessários, resultando assim numa redução de emissões de carbono. Para além de serem renováveis, estes materiais fornecem benefícios por serem biodegradáveis e renováveis.

Na sua forma mais simples uma sandwich estrutural é composto por duas faces finas e rígidas e um núcleo leve e espesso colocado entre as mesmas. As propriedades de interesse primário para os materiais do núcleo podem ser resumidas da seguinte forma: baixa densidade, módulo de corte elevado, resistência ao corte elevada, rigidez elevada na direção normal às faces e boas características isolantes tanto termicamente como acusticamente. Os materiais de núcleo frequentemente usados são espumas, balsa e estruturas em forma de favo de abelha, que consistem em estruturas superleves com elevadas razões de resistência-peso e rigidez-peso. A configuração favo de abelha pode ser definida como sendo uma matriz de células abertas, formadas a partir de folhas de materiais apropriados, ligadas entre si em intervalos controlados e depois expandidos em ordem a formar células hexagonais. No entanto, desenvolvimentos recentes resultaram em novas alternativas, tais como estruturas de núcleo celular que é o caso da cortiça. A cortiça tem uma estrutura celular alveolar similar ao da configuração de favo de abelha e as suas células são principalmente compostas por suberina, lenhina e celulose. Embora pareça que cortiça natural tenha um fraco comportamento mecânico quando comparado a outros tipos de materiais de núcleo, tais como espumas sintéticas, para algumas aplicações específicas, a cortiça consegue mesmo competir com estes materiais. A sua baixa condutividade térmica combinada com a sua resistência à compressão razoável torna a cortiça um excelente material para propósitos de isolamento térmico como também para aplicações em que estão presentes cargas de compressão.

O trabalho aqui apresentado visa estudar a viabilidade de implementar cortiça, mais especificamente o aglomerado de cortiça NL20 fabricado por Amorim Cork Composites, como o material de núcleo de estruturas sandwich com faces de alumínio (Aalco 5754) caracterizando termicamente nove provetes de painéis sandwich circulares através de ensaios experimentais. Tendo em conta os desafios enormes impostos pelos *stake-holders* globais de reduzir

drasticamente (75% por passageiro/km) o impacto ambiental, tais como as emissões de CO₂, associadas às tecnologias de fabricação, bem como de operação e manutenção atuais dos vários tipos de transporte, torna-se fundamental que a indústria aeronáutica comece por incorporar uma quantidade elevada de componentes recicláveis, para além de mais leves. Sendo assim, um dos objetivos chave deste estudo é reduzir o peso dos provetes mantendo as suas características térmicas ao aplicar diferentes padrões de furo nos seus núcleos de cortiça. Os configurações de núcleo diferem em forma do furo, diâmetro e profundidade de forma a que a influência destes fatores pudesse ser estudada. No entanto, é incluído um provete uniforme que irá servir de modelo de referência para os restantes. O efeito que a massa de cortiça tem na capacidade isolante também foi estudada. Estes provetes, todos eles isolados termicamente lateralmente de forma a assegurar o fluxo de calor unidimensional, foram aquecidos a 80 °C na face inferior e a sua capacidade isolante individual foi determinada através da medição da temperatura no centro da face superior com um termopar de contacto. A distribuição de temperatura nas faces superiores também foi registada através de uma câmara termográfica de infravermelhos posicionada acima dos provetes. As análises numéricas foram realizadas recorrendo ao código de elementos finitos ABAQUS® v6.10-1. Os ensaios experimentais tiveram que ser realizados em primeiro de forma a determinar o coeficiente convectivo experimental para posteriormente ser usado nas análises numéricas. A transferência de calor através de radiação foi provada como tendo muito pouca influência nos resultados devido às diferenças de temperatura reduzidas entre os provetes e a vizinhança, pelo que é praticamente desprezável.

As conclusões tiradas a partir da comparação entre os resultados experimentais e numéricos permitem dar um passo importante no sentido da adoção de cortiça como o material de seleção para o núcleo de estruturas sandwich e deverão servir como base ou referência para estudos futuros mais detalhados nesta área.

Palavras-Chave: Cortiça; Estruturas Sandwich; Caracterização térmica; Análise Numérica; Capacidade Isolante; Padrões de Furos

Contents

Acknowledgements	v
Abstract	ix
Resumo	xiii
Contents	xvii
List of Figures.....	xxi
List of Tables.....	xxv
Acronyms	xxvii
Chapter 1 - Introduction	1
1.1 Motivation	1
1.1.1 Advantages.....	2
1.1.2 Facing Materials.....	3
1.1.3 Core Materials.....	4
1.1.3.1 Foams	5
1.1.3.2 Honeycomb.....	6
1.1.4 Manufacture and Applications.....	9
1.2 Historical Background	12
1.3 Objectives	15
1.4 The DesAir Project	17
1.5 Previous Work.....	19
Chapter 2 - Cork and its properties.....	21
2.1 Cork Morphology.....	21
2.2 Ecological and economic importance.....	25
2.3 Cork Agglomerates	27
Chapter 3 - Experimental Characterization.....	29
3.1 Manufacture of the test samples.....	29
3.2 Experimental Setup	40
Chapter 4 - Numerical modeling of Sandwich Panels	43
4.1 Numerical model description	43
4.2 Mesh Convergence Study.....	54
Chapter 5 - Results and discussion.....	59
5.1 Experimental Results	59
5.2 Numerical Results	64
Chapter 6 - Conclusions and future research	71
6.1 Final conclusions	71
6.2 Prospects for future developments	72
References	75

Annex A - Sandwich material properties 79
Annex B - Numerical simulation results 82

List of Figures

Figure 1 - Sandwich Construction (Bitzer, 1997)	1
Figure 2 - Construction of a sandwich panel compared to an I beam. (Hexcel Composites, 2000)	1
Figure 3 - Relative Stiffness, strength and weight of sandwich panels compared to a solid laminate. (Hexcel Composites).....	3
Figure 4 - Hexagonal honeycomb cells (Bitzer, 1997).....	4
Figure 5 - Types of Sandwich Construction (Vinson, 1999)	5
Figure 6 - Honeycomb density types (a) (FAA, 2012).....	7
Figure 7 - Honeycomb density types (b) (FAA, 2012).....	8
Figure 8 - Honeycomb density types (FAA, 2012)	8
Figure 9 - Corrugated core sandwich used in packaging boxes (Carlsson, 2011).	9
Figure 10 - Examples of Sandwich applications on the Airbus A380 (Herrmann, 2005)	9
Figure 11 - VTP major structural assemblies (example A380). (Herrmann, 2005)	10
Figure 12 - Fuselage of the De Havilland Mosquito (Herrmann, 2005)	13
Figure 13 - DesAir logo	17
Figure 14 - Diagram of the three-dimensional structure of cork. (Pereira, 2007)	21
Figure 15 - Schematic representation of axial section of cork oak tree; (A) cork (suberose tissue), (B) subero-phellogenic change, (C) phellogenium, (D) liber tissue, (E) liberwood change, (F) wood, (G) bark, (H) lenticular channels, (I) area for stopper production, (J) annual growth rings (Silva, S.P. & Sabino, 2005)	22
Figure 16 - Micrograph of natural cork (after boiling) obtained through SEM (Silva, S.P. & Sabino, 2005)	23
Figure 17 - The growth process of cork (Gil, 2007).....	25
Figure 18 - Cork Agglomerates Types (Mestre, A. & Gil. L, 2011).....	27
Figure 19 - Aalco 5754 square aluminum face sheets	29
Figure 20 - Bi-metal 152 mm hole saw.....	29
Figure 21 - Milling machine with hole saw	30
Figure 22 - Cutting process of the aluminum sheet.....	30
Figure 23 - Extracted Aluminum face sheet.....	31
Figure 24 - Original NL20 Cork agglomerate plate	31
Figure 25 - Preview of the cork plate with drilling patterns developed in CATIA®	31
Figure 26 - Development of the drilling patterns	32
Figure 27 - Finished Cork Plate with drilling patterns and profile cuts	32
Figure 28 - Rendering of the finished cork plate designed in CATIA®.....	33
Figure 29 - Small tab that prevents any movement by the cork sample.....	33
Figure 30 - Extracted Cork Samples	34
Figure 31 - Glue componentes (A and B)	35

Figure 32 - Application of the glue mixture.....	35
Figure 33 - Final assemblies after curing process.....	36
Figure 34 - Top face sheet edge before smoothing.....	36
Figure 35 - Top face sheet edge after smoothing.....	36
Figure 36 - Fully expanded polyurethane foam	38
Figure 37 - First mold version (without cover)	38
Figure 38 - New molds with holes (open).....	38
Figure 39 - New mold with cover and clamps (closed).....	38
Figure 40 - Closed molds with fully expanded foam.....	39
Figure 41 - Test samples after removing the mold cover.....	39
Figure 42 - Finished laterally insulated test samples	39
Figure 43 - Test samples placed on heating plate	40
Figure 44 - Alternating current transformer	40
Figure 45 - Contact thermocouple.....	41
Figure 46 - Thermographic camera placed directly above the test samples.....	41
Figure 47 - Infrared thermal imaging system Thermo Tracer TH1100.....	41
Figure 48 - Complete experimental setup.....	42
Figure 49 - 1 mm thick aluminum face sheet.....	44
Figure 50 - Cores of the uniform model and the bracket hole model (l. to r.)	44
Figure 51 - The 5.14 mm, 7 mm and 10 mm hole models (l. to r.)	45
Figure 52 - Non-through hole models without offset and with offset (l. to r.)	45
Figure 53 - The 6mm models intended for the mass study.....	46
Figure 54 - Isometric view of the completely partitioned models	47
Figure 55 - Frontside and backside tie constrains (l. to r.)	47
Figure 56 - Highlighted surface for backside face sheet heating.....	48
Figure 57 - Selection of the thermally insulated side of the model	48
Figure 58 - Highlighted surface for convective heat transfer.....	49
Figure 59 - Layout of the experimental setup with the heating plate and the sample	50
Figure 60 - Hexahedral (l.), wedge (m.) and tetrahedral (r.) element meshes	52
Figure 61 - Core mesh convergence study with 171533 (l.), 270712 and 444728 elements (r.) 54	
Figure 62 - Face sheet mesh convergence study with 335202 (l.), 341058 and 365746 (r.) elements.....	55
Figure 63 - Core and face sheet mesh convergence study	56
Figure 64 - Temperature measurement of the heating plate	59
Figure 65 - Temperature measurement of the test samples.....	59
Figure 66 - Bar chart of the experimental results	60
Figure 67 - Thermographic image taken from the infrared camera above	61
Figure 68 - Thermographic image with temperature range up to 40° C.....	62
Figure 69 - Thermographic image with temperature range up to 42° C.....	62
Figure 70 - Bar chart of the numerical and experimental results.....	65

Figure 71 - Temperature distributions for the uniform, non-through hole with offset, and 10 mm circular hole models (l. to r.)	66
Figure 72 - Outer and inner sides of the front side face sheet	66
Figure 73 - Temperature layer evolution through the thickness of the core.....	67
Figure 74 - Temperature profiles through the thickness of each model	68
Figure B. 1 - Numerical results for the uniform model	82
Figure B. 2 - Numerical results for the bracket model.....	82
Figure B. 3 - Numerical results for the 5.14 mm circular hole model	83
Figure B. 4 - Numerical results for the 6 mm circular hole model (a) (light version).....	83
Figure B. 5 - Numerical results for the 6 mm circular hole model (b) (heavy version)	84
Figure B. 6 - Numerical results for the 7 mm circular hole model	84
Figure B. 7 - Numerical results for the non through hole model without offset	85
Figure B. 8 - Numerical results for the non through hole model with offset	85
Figure B. 9 - Numerical results for the 10 mm circular hole model.....	86

List of Tables

Table 1 - General mechanical properties of cork (Silva, S.P. & Sabino, 2005)	24
Table 2 - Weight and expected weight values for the core samples	34
Table 3 - Weight and expected weight values for the top and bottom face sheets	35
Table 4 - Final assembly weight compared to the combined weight of the individual parts ..	37
Table 5 - Final assembly weight compared to the expected weight from the numerical analysis	37
Table 6 - Model description and study purposes	46
Table 7 - Temperature outputs and mesh convergence study for the 7mm model	55
Table 8 - Core mesh convergence study of the non-through hole model without offset	57
Table 9 - Calculated convective heat transfer coefficient for each test sample.....	64
Table 10 - Numerical Results versus Experimental Results.....	65
Table A. 1 - Properties of typical facing materials for sandwich panel construction (Hexcel Composites, 2000).....	79
Table A. 2 - Balsa wood and some commonly used foam core material systems. (Beckwith, 2008)	80
Table A. 3 - Comparison of core material relative costs and their characteristics and benefits. (Beckwith, 2008)	80
Table A. 4 - Mechanical Properties of Honeycomb Materials - Typical Values at Room Temperature (Hexcel Composites, 2000).....	81

Acronyms

QREN	Quadro de Referência Estratégica Nacional
ACC	Amorim Cork Composites
SEM	Scanning electron microscopy
VTP	Vertical Tail Plane
R	Radial direction
NR	Non radial direction
DAI	DynAero Iberica
ASTM	American Society for Testing and Materials
CNC	Computer Numerical Controlling

Chapter 1 - Introduction

1.1 Motivation

By Carlsson's definition, a structural sandwich typically consists of two thin "face sheets" made from stiff and strong relatively dense material such as metal or fiber composite bonded to a thick lightweight material called "core" (Carlsson, 2011).

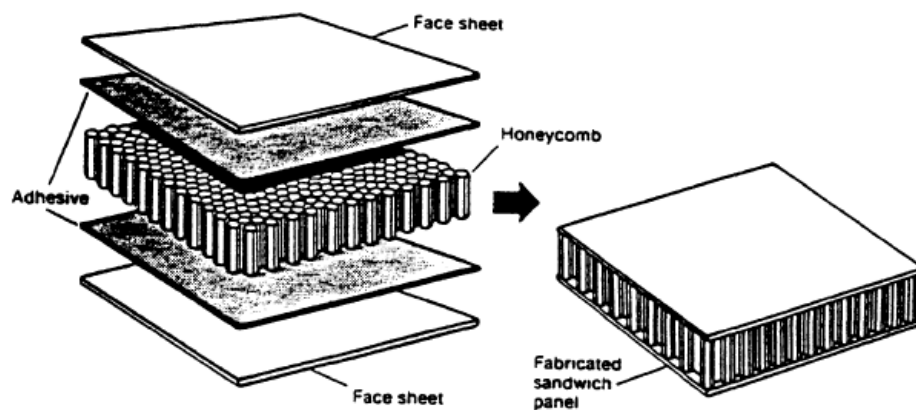


Figure 1 - Sandwich Construction (Bitzer, 1997)

The facing skins of a sandwich panel mimic the flanges of an I-beam, as they carry the bending stresses to which the beam is subjected (figure 2). With one facing skin under compression, the other is under tension. A similar comparison can be made between the honeycomb core and the web of the I-beam.

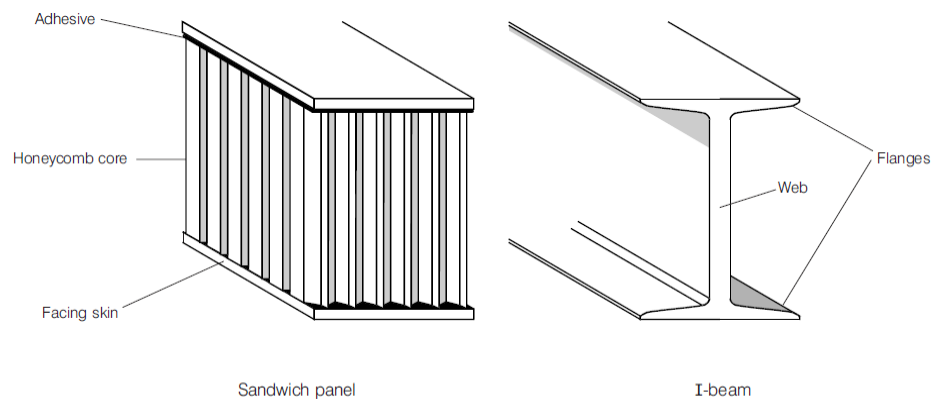


Figure 2 - Construction of a sandwich panel compared to an I beam. (Hexcel Composites, 2000)

The core resists the shear loads and increases the stiffness of the structure by holding the facing skins apart, and improving on the I-beam. It gives continuous support to the flanges or facing skins to produce a uniformly stiffened panel. The core-to-skin adhesive rigidly joins the sandwich components and allows them to act as one unit with a high torsional and bending rigidity (Hexcel Composites, 2000).

Sandwich is a common principle in nature. The branches of the elder tree are a good example for a foam core sandwich structure. The bones in the skeletons of animals and humans are sandwich structures with foam-like core materials as well. Natural sandwich structures are subjected to complex load cases. The bones in legs have to withstand repetitive, super positioned bending and compression loads. Moreover nature imposes a strict demand for lightweight primary structures, such as skeletons of birds. All the mentioned examples show the principle of structural optimization which is the minimum use of material for maximum performance (Herrmann, 2005).

1.1.1 Advantages

Sandwich structures allow optimizing structures that are weight-critical such as aircraft components, space structures, sporting goods, naval structures, and blades for wind-power generation. Besides providing a very efficient load-carrying structure, the sandwich concept enables design of multi-functional structures. They also possess a high resistance to fatigue from jet efflux. However, in special cases the faces may differ in either thickness, material or both, because one face may be the primary load-carrying, low-temperature portion while the other face must withstand an elevated temperature, corrosive environment, etc. (Vinson, 1999). The sandwich is not a material having unique mechanical properties; rather, it is a structure which must be designed for the particular uses to which it will be subjected.

Sandwich construction is playing an increasingly important role in structures because of its exceptionally high flexural stiffness-to-weight ratio compared to monocoque and other architectures. As a result, sandwich construction results in lower lateral deformations, higher buckling resistance, and higher natural frequencies. Thus, for a given set of mechanical and environmental loads, sandwich construction often results in a lower structural weight than do other configurations. Sandwich structures represent a key component of composites structural design technology. The core materials selected for the center of the sandwich structure come in a variety of material types, forms and properties (both mechanical and physical). The end-use application very often dictates which material is best for the resultant structural application and the composition of the sandwich is limited only by the availability of materials and the engineer's ingenuity (Beckwith, 2008). The principal advantage of sandwich panels is that the rigidities can take any values in function of geometrical parameters. Thus, the designer

has the choice for optimizing the material solution (Vamja, 2012). Sandwich construction has high bending stiffness at minimal weight in comparison to aluminum and composite laminate construction. Most honeycombs are anisotropic; that is, properties are directional. Figure 3 shows the advantages of using a honeycomb construction.


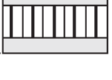

	Solid Material	Core Thickness t	Core Thickness $3t$
			
Stiffness	1.0	7.0	37.0
Flexural Strength	1.0	3.5	9.2
Weight	1.0	1.03	1.06

Figure 3 - Relative Stiffness, strength and weight of sandwich panels compared to a solid laminate. (Hexcel Composites)

Increasing the core thickness greatly increases the stiffness of the honeycomb construction, while the weight increase is minimal. Due to the high stiffness of a honeycomb construction, it is not necessary to use external stiffeners, such as stringers and frames (FAA, 2012).

1.1.2 Facing Materials

Most honeycomb structures used in aircraft construction have aluminum, fiberglass, Kevlar®, or carbon fiber face sheets. Carbon fiber face sheets cannot be used with aluminum honeycomb core material, because it causes the aluminum to corrode. Titanium and steel are used for specialty applications in high temperature constructions. The face sheets of many components, such as spoilers and flight controls, are very thin—sometimes only 3 or 4 plies. Field reports have indicated that these face sheets do not have a good impact resistance (FAA, 2012). Du reports that Carbon fiber-reinforced polymer (CFRP) composites and glass fiber-reinforced polymer (GFRP) composites are the most widely used skin materials for sandwich panels (Du, 2012). Some properties of typical facing materials for sandwich panel construction are shown in table A. 1 in Annex A.

1.1.3 Core Materials

As already mentioned, the primary function of the core is to stabilize the outer skins, although it may be stress bearing as well. Carlsson classifies core materials within two broad categories: “cellular” and “structural”. The former implies that the material consists of “cells” containing open space enclosed by walls in a repetitive manner so that space filling is achieved (figure 4). Cellular foams, such as polymer or metal foams, honeycomb core, and balsa wood, are very common in structural applications. Web core on the other hand is a structural core that consists of a continuous web made from a solid material formed in such a way that it separates the faces and becomes effective in transferring shear forces (Carlsson, 2011).

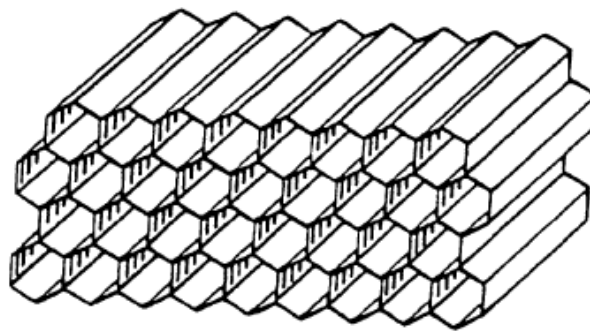


Figure 4 - Hexagonal honeycomb cells (Bitzer, 1997)

Vinson however states that in general cores fall into four types: (a) foam or solid core, (b) honeycomb core, (c) web core, and (d) a corrugated or truss core (see figure 5). In most foam-core and honeycomb-core sandwiches one can assume that all of the in-plane and bending loads are carried by the faces only. However, in web-core and truss-core construction, a portion of the in-plane and bending loads are also carried by the core elements. Web core construction is also analogous to a group of I-beams with their flanges welded together. In the web core and truss core (or triangulated core) constructions, the space in the core could be used for liquid storage or as a heat exchanger. In the present thesis only foam-core and honeycomb-core sandwich constructions will be covered with more detail. Their primary purpose is to insure the spacing between the faces and to carry the transverse shear loads to which the structure is subjected. Also, generally, the core is a very small percentage of the sandwich weight (Vinson, 1999). Core material families exhibit a wide range of material costs, advantages and disadvantages across the applications spectrum. Table A. 2 and Table A. 3 in Annex A explore a few of these factors for each family given above (Beckwith, 2008).

1.1.3.1 Foams

Foam or solid cores are relatively inexpensive and can consist of balsa wood, and an almost infinite selection of foam/plastic materials with wide truss core constructions, the space in the core could be used for liquid storage or as a heat exchanger. Balsa is a natural wood product with elongated closed cells, available in a variety of grades that correlate to the structural, cosmetic, and physical characteristics. Although the density of balsa is less than one-half of the density of conventional wood products, it has a considerably higher density than the other types of structural cores. (FAA, 2012). Foam cores are used on homebuilt and lighter aircraft to give strength and shape to wing tips, flight controls, fuselage sections, wings, and wing ribs. Foam cores are not commonly used on commercial type aircraft. Foams are typically heavier than honeycomb and not as strong.

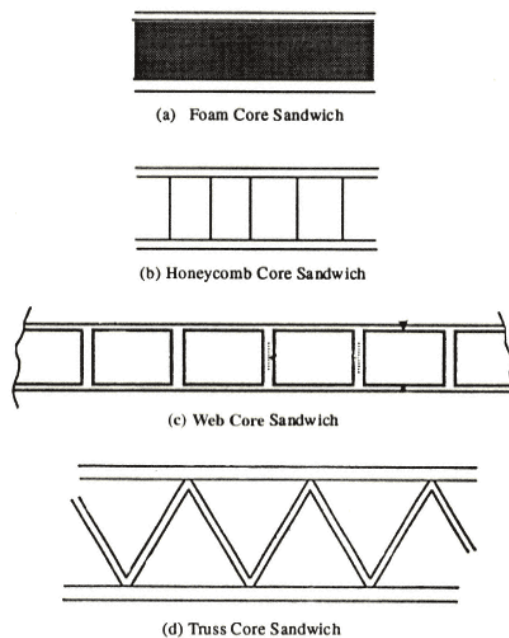


Figure 5 - Types of Sandwich Construction (Vinson, 1999)

A variety of foams can be used as core material including (Vinson, 1999), (FAA, 2012):

- **Polystyrene (expanded, EPS and extruded, XPS)** - Aircraft grade Styrofoam with a tightly closed cell structure and no voids between cells; A thermoplastic material with high compressive strength and good resistance to water penetration; can be cut with a hot wire to make airfoil shapes;
- **Phenolic** – A thermosetting material; not yet widely used; very good fire-resistant properties and can have very low density, but relatively low mechanical properties;
- **Polyurethane** – Another thermosetting material, this one however is widely used for producing the fuselage, wing tips, and other curved parts of small aircraft; relatively

inexpensive, fuel resistant, and compatible with most adhesives; no hot wire cut allowed; easily contoured with a large knife and sanding equipment;

- **Polypropylene** – used to make airfoil shapes; can be cut with a hot wire; compatible with most adhesives and epoxy resins; not for use with polyester resins, dissolves in fuels and solvents;
- **Polyvinyl chloride (PVC)** – a closed cell medium-to-high-density foam with high compression strength, durability, and excellent fire resistance; can be vacuum formed to compound shapes and be bent using heat; compatible with polyester, vinyl ester, and epoxy resins. Examples are Divinycell[®], Klegecell[®], and Airex[®];
- **Polymethacrylimide (Rohacell)** – a closed-cell foam used for lightweight sandwich construction; excellent mechanical properties, high dimensional stability under heat, good solvent resistance, and outstanding creep compression resistance; more expensive than the other types of foams, but has greater mechanical properties.

1.1.3.2 Honeycomb

Each honeycomb material provides certain properties and has specific benefits. The most common core material used for aircraft honeycomb structures is aramid paper (Nomex[®] or Korex[®]). Fiberglass is used for higher strength applications. Some of the honeycomb materials used as core material include (Hexcel Composites, 2000), (FAA, 2012):

- **Kraft paper** – Relatively low strength, good insulating properties, is available in large quantities, and has a low cost;
- **Thermoplastics** – Good insulating properties, good energy absorption and/or redirection, smooth cell walls, moisture and chemical resistance, are environmentally compatible, aesthetically pleasing, and have a relatively low cost;
- **Aluminum** – Best strength-to-weight ratio and energy absorption, has good heat transfer properties, electromagnetic shielding properties, has smooth, thin cell walls, is machinable, and has a relatively low cost;
- **Steel** – Good heat transfer properties, electromagnetic shielding properties, and heat resistant;

- **Titanium** – relatively high strength-to-weight ratio, good heat transfer properties, chemical resistance, and heat resistant to very high temperatures;
- **Aramid paper** – Flame resistant, fire retardant, good insulating properties, low dielectric properties, and good formability;
- **Fiberglass** – Tailorable shear properties by layup, low dielectric properties, good insulating properties, and good formability;
- **Carbon** – Good dimensional stability and retention, high-temperature property retention, high stiffness, very low coefficient of thermal expansion, tailorable thermal conductivity, relatively high shear modulus, but very expensive;
- **Ceramics** – Heat resistant to very high temperatures, good insulating properties, is available in very small cell sizes, and very expensive.

Selected mechanical properties for Aluminum and Nomex[®] honeycombs are shown in Table A. 4 in Annex A. Honeycomb core cells for aerospace applications are usually hexagonal, see figure 6. The cells are made by bonding stacked sheets at special locations.

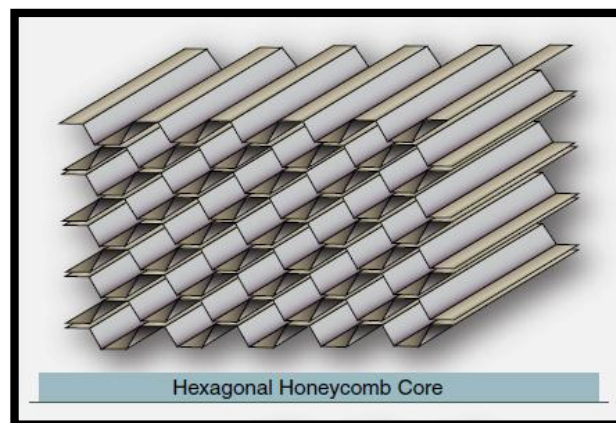


Figure 6 - Honeycomb density types (a) (FAA, 2012)

The stacked sheets are expanded to form hexagons. The direction parallel to the sheets is called ribbon direction. Bisected hexagonal core has another sheet of material cutting across each hexagon. Bisected hexagonal honeycomb is stiffer and stronger than hexagonal core. Over expanded core is made by expanding the sheets more than is needed to make hexagons.

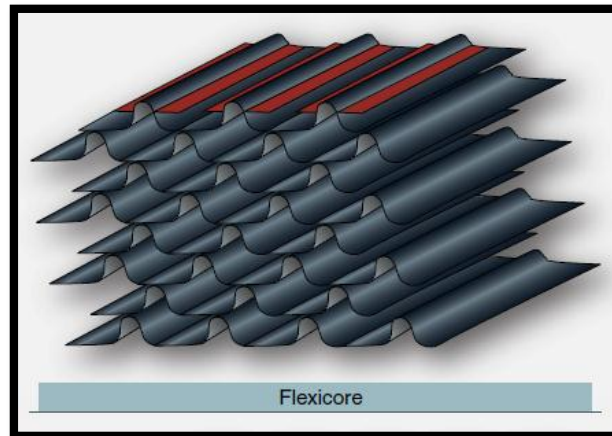


Figure 7 - Honeycomb density types (b) (FAA, 2012)

The cells of over expanded cores are rectangular. Over expanded cores are flexible perpendicular to the ribbon direction and used in panels with simple curves. Bell-shaped core, or flexi core, has curved cell walls that make it flexible in all directions, see figure 7.

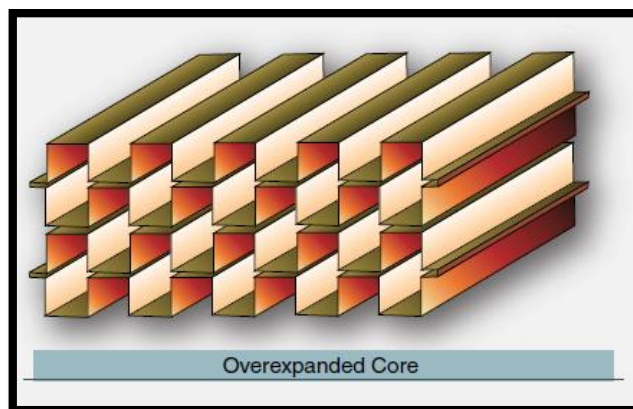


Figure 8 - Honeycomb density types (FAA, 2012)

Bell-shaped core is used in panels with complex curves. Honeycomb core is available with different cell sizes. Small sizes provide better support for sandwich face sheets. Honeycomb is also available in different densities. Higher density core is stronger and stiffer than lower density core (FAA, 2012).

1.1.4 Manufacture and Applications

Composite sandwich construction is most often fabricated using autoclave cure, press cure, or vacuum bag cure. Skin laminates may be pre-cured and subsequently bonded to the core, co-cured to the core in one operation, or a combination of the two methods. The sandwich concept has long been utilized in packaging materials, such as corrugated paper board (figure 9).

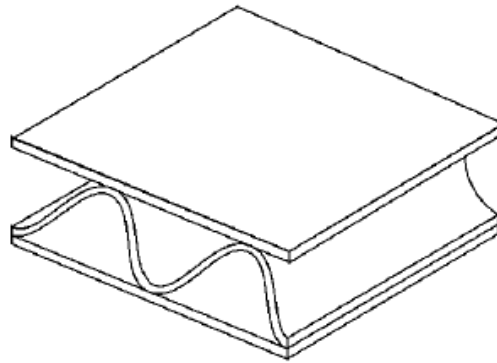


Figure 9 - Corrugated core sandwich used in packaging boxes (Carlsson, 2011).

The uses of this method of construction include lightweight “planks” for cabin furniture, monolithic fairing shells generally having plastic facing skins, and the stiffening of flying control surfaces. Thus, for example, the ailerons and rudder of the British Aerospace Jaguar are fabricated from aluminum honeycomb, while fiberglass- and aluminum-faced honeycomb are used extensively in the wings and tail surfaces of the Boeing 747. Some problems, mainly disbonding and internal corrosion, have been encountered in service (Megson, 2010).

There is a broad range of composite sandwich structures application in Airbus aircraft. Typical external structures are aerodynamic fairings, covers and doors. Examples are radomes, belly fairings, leading and trailing edge fairings, engine cowlings and landing gear doors. Moreover, there is a variety of composite sandwich control surfaces throughout the Airbus fleet (e.g. rudder, aileron, spoiler).

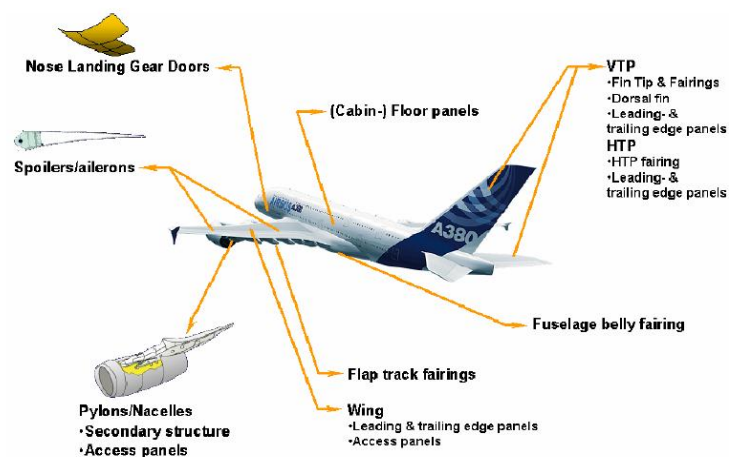


Figure 10 - Examples of Sandwich applications on the Airbus A380 (Herrmann, 2005)

Examples for the application of composite sandwiches inside the aircraft are fairings and floor panels in the passenger compartment. Figure 10 gives an overview of composite sandwich applications in the A380 aircraft (Herrmann, 2005). To fulfill the different requirements a variety of material combinations can be found in the current composite sandwich structures. Predominantly, skin materials include glass fiber and carbon fiber reinforced preregs with epoxy resin matrices whereas the core materials for sandwiches include NOMEX® honeycomb. Due to fire, smoke and toxicity requirements (FST) less hazardous phenolic resins are being applied in the manufacture of surface layers of cabin interiors. ROHACELL® PMI hard foam is being applied as a manufacturing aid (lost tool; e.g. hat profiles for A340 and A380 rear pressure bulkhead). Vertical tail planes of Airbus aircraft consist of 5 major structural assemblies (figure 11):

1. Leading edge fairings (including tip and dorsal fin)
2. Center box structure (including the interface to the fuselage)
3. Trailing edge fairings
4. Rudder
5. Fin - fuselage fairing

For the A340 VTP, the center box structure is the only structural assembly that is not produced with composite sandwiches.



Figure 11 - VTP major structural assemblies (example A380). (Herrmann, 2005)

The leading edge fairings (including tip and dorsal fin) have to withstand aerodynamic loads, abrasion and hail-, bird- and lightning strike. Antennas are mounted behind the leading edge and the tip, therefore they have to allow for electromagnetic transmission. The Material combination for these areas is glass fibre reinforced prepreg and NOMEX® honeycomb. The

largest sandwich structure in the A340 VTP is the rudder. It consists of the following major components (Herrmann, 2005):

- Left and right hand skin panel (NOMEX® honeycomb and carbon fibre prepreg; layers of glass fibre prepreg in specific areas for corrosion protection)
- Front spar (monolithic carbon fibre prepreg)
- Root rib (monolithic carbon fibre prepreg)
- Diverse fittings (aluminium parts)
- Diverse small parts

Sandwich is the ideal structure for this large component as stiffness to weight ratio is a critical requirement for control surfaces.

1.2 Historical Background

As one of the most effective construction designs for increasing the stiffness-to-weight ratio, sandwich structures are said to be envisioned by Da Vinci, (Allen, 1993). Noor, Burton, and Bert, (Noor, 1996), and Bitzer, (Bitzer, 1997), report in their work that one of the earliest man-made sandwich structures goes back to Fairbairn, who described the sandwich construction principle in 1849 for the Britannia Tubular Bridge in North Wales, built in 1845, which consisted of a large rectangular tube, the floor of which supported railroad tracks, and through which trains ran (Fairbairn, 1849). The tube's top compressive panel had two flat plates connected to a square cell eggcrate type wood core. One of the earliest known honeycomb core patents, covering a manufacturing method for the production of Kraft paper honeycomb, is the Budwig Patent, issued in 1905 in Germany. It was not until 1919 that the first aircraft sandwich panel was fabricated using thin mahogany facings bonded to an end-grain balsa wood core. It was used as the primary structure of the pontoons of a seaplane.

Bitzer also states that, between World War I and World War II, plywood skins glued to a balsa wood core were used as the primary structure in Italian seaplanes. An entire squadron of these aircraft was flown to Brazil in the 1920s and another squadron was flown to the Chicago World's Fair in the 1930s which was truly a remarkable demonstration of flight time for that period. The manufacture of modern structural honeycombs only began in the late 1930s when J. D. Lincoln manufactured Kraft paper honeycomb for use in the furniture built by Lincoln Industries in Marion, Virginia, USA. The material was used in sandwich panels which consisted of thin hardwood facings bonded to a relatively thick slice of paper honeycomb.

At the outbreak of World War II paper honeycomb was used by the Glen L. Martin Company in radomes - structural enclosures for radar antennas, which were then in their infancy and became quite successful. However, the paper core did pick up moisture. Martin later developed a honeycomb made of cotton duck fabric and by the end of World War II they had produced honeycomb cores made of cotton fabric, glass fabric and aluminum foil. The chief designer of De Havilland, E. Bishop, was the first person to use the sandwich principle in a powered aircraft. He used the sandwich concept in the fuselage of the Comet Racer, the Albatross and in the wing and fuselage of their successor, the famous Mosquito, illustrated in figure 12 (Herrmann, 2005).

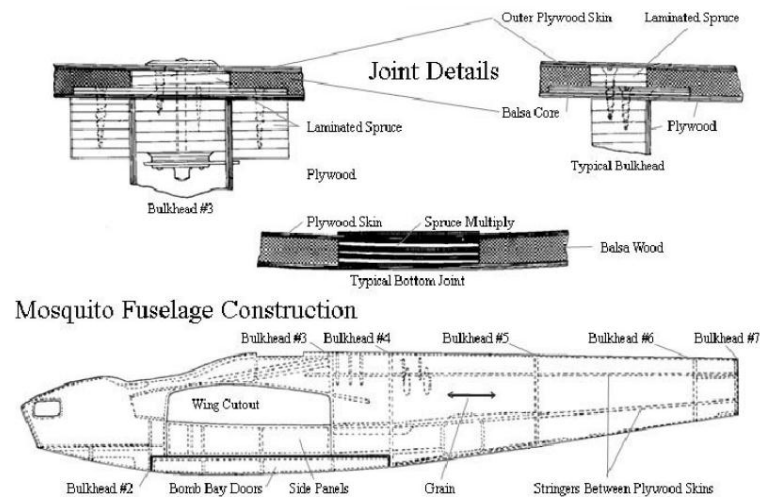


Figure 12 - Fuselage of the De Havilland Mosquito (Herrmann, 2005)

The excellent performance displayed by this airplane led to the acceptance of many aircraft designers, particularly in England, of the basic superiority of the sandwich structure as a means of making a more efficient and higher performing airplane. As a result many aircraft design groups began to examine better ways to make sandwich structures and better materials from which to make the cores and facings. It was not until 1945 that the first all-aluminum sandwich panel was produced. In the late 1940s, two young World War II veterans formed Hexcel Corporation, which over the decades has played the most important role of any firm in the growth of sandwich structures. Starting with honeycomb cores, even today they make well over 50% of the world's honeycomb core materials, states Vinson, (Vinson, 2005). Also, in 1948, Hoff, (Hoff, 1950), derived the differential equations and boundary conditions for the bending and buckling of sandwich plates using the principle of virtual displacements, but pursued only the buckling problem of panels under edgewise compression. In the same year, Libove and Batdorf, (Libove, 1948), published a general small deflection theory for sandwich plates.

The real breakthrough came with the development of better adhesives for the attachment of facings to the cores. Adhesives were developed that had the right rheology, which consists of the flow during curing, for use with honeycomb. The adhesives stayed on the honeycomb cell edges when the facings were being bonded. Earlier adhesives would not stay on the top honeycomb surface but instead ran down the cell walls. Therefore, it was not possible to achieve a good bond to the top skin. In this period of time most adhesives gave off volatiles when curing so the aluminum honeycomb cores had to be perforated (small pin holes put in the foil before being made into core) to allow the gases to escape during cure. If the core was not perforated the buildup of pressure within the cells could prevent a good core-to-facing bond and even blowout the core. Now most modern adhesives are 100% solids and do not give off volatiles. Thus, honeycombs don't need to be perforated anymore. Currently, the sandwich core is usually perforated for space applications where air is not wanted in the cells.

By the mid-1960s, efforts in sandwich research had spread widely. In 1966, Plantema published his famous, and the first, book on sandwich structures (Plantema, 1966). In 1969, this was followed by the book by H.G. Allen, (Allen, 1969). These books were the "bibles" for sandwich structures for many years. In 1989, Ha provided an overview of finite elements applied to sandwich plates, (Ha, 1989). Two years later, Bert provided a review of sandwich plate analysis (Bert, 1991). In 1999, the Journal of Sandwich Structures and Materials was initiated and it is the only Journal fully devoted to sandwich structures and Materials. Vinson reports that over 180 research papers have been published in the journal to date (Vinson, 2005).

Today, Europe is the leader in the use of sandwich constructions for lightweight railcars, while in the U.S. some of the rapid transit trains use honeycomb sandwich, as stated by Vinson, (Vinson, 1999). The U.S. Navy is using honeycomb-sandwich bulkheads to reduce the ship weight above the waterline. Sailboats, racing boats, and auto racing cars are all employing sandwich construction. Sandwich construction is also used in snow skis, water skis, kayaks, canoes, pool tables, and platform tennis paddles.

1.3 Objectives

The present thesis is essentially subdivided in two distinct parts which will ultimately be compared to each other in order to draw the proper conclusions. The main objective is to assess the viability of using a specific type of cork agglomerate as the core material of a sandwich structure with aluminum face sheets. Nine circular sandwich panels were heated up to 80 °C on the lower face sheet and the temperature on the center of the top face sheet was measured in order to determine the overall insulating ability of the sandwich configuration. Nine samples with different core configurations were tested.

Although the first section corresponds to the experimental procedures, some computational work had to be done before that in order to design and develop the core configurations. The core configurations differ in hole shape, diameter, depth and cork mass. Each set of cores was specifically designed so that their impact on the insulating ability could be assessed. The hole diameters and the spacing between holes were established so that all the models had the same mass, except for the uniform model and a pair of 6 mm circular hole models. This had to be done using a trial and error methodology on ABAQUS® v6.10-1. As mentioned earlier, the first model is the uniform model which has no hole pattern in its core and will serve as reference to all the remaining models. The objective here is to investigate if and to which point the presence of the holes, or the lack of cork, compromises the thermal characteristics by comparing the models to the uniform configuration. Between the models with the same mass, there is a model with holes in its core that resemble brackets, thus being called the bracket model. It is intended to study the influence of the hole shape with this model. There are three models with the same cork mass, the same hole shape but different hole diameters (5.14 mm, 7 mm and 10 mm), which are the circular hole models. By keeping the mass constant, the effect of the hole diameter on the insulating ability is intended to be investigated. Although the two 6 mm hole models have the same circular hole shape, their masses differ. The “a” version has less mass than the other models and the “b” version has more. Nevertheless, the heaviest model remains the uniform model. The objective here is to study how the insulating ability varies with the cork mass. The last two models are a pair of non through hole models. Although they have the same circular hole shape, their thickness is essentially partitioned in three sections, where the middle section is a 6 mm thick cork partition, leaving a hole with a depth of 6 mm on each side. These models were tested in order to study the difference in results between a through hole model and a non through hole model. However, they were also compared to each other given that one has a 6 mm offset between the holes on each side. Therefore, the effect of the offset was assessed. The experimental procedures in the first section are comprised by two subsections, the first one being a detailed description of the manufacture of the test samples and in the second the experimental setup will be explained.

In the second part in which this thesis is subdivided, numerical simulations were performed which were validated by the results from the experimental tests afterwards. The numerical simulations were carried out resorting once again to the finite element code ABAQUS® v6.10-1. As mentioned earlier, the experimental tests had to be performed first so that the experimental convective heat transfer coefficient could be determined and subsequently used in the numerical simulations in order to obtain more exact results. A description of the numerical models is given along with an explanation of the material properties, section definition types, boundary conditions, interactions as well as the simplifications made during the simulations. A mesh convergence study was performed for some models in order to find the right element number for the mesh. Finally, the results extracted from the experimental tests are compared to those of the numerical simulations in order to identify the best core configurations and to determine the magnitude and effect of the aforementioned core configuration factors.

1.4 The DesAir Project

The DesAIR project, in which this work is inserted, has the objective of developing new high performance composite solutions intended to be applied in aircraft interiors, integrating natural materials and developing specific manufacturing processes. The solutions currently in use, such as reinforcement fibres with a thermosetting polymeric matrix, present several problems in their sustainability. In order to solve these problems and using a coherent and systematic scientific approach, the use of entirely natural materials will be studied and developed. The new material integration and manufacturing processes will also be tested in this project and further validated in a demonstrator representative of interior parts/components of commercial or executive aircrafts (Desair, 2012).



Figure 13 - DesAir logo

The main motivation of this project is linked to the need of answering the enormous challenges imposed by the global stake-holders of reducing drastically (75% per passenger/km) the environmental impact, such as the CO₂ emissions, associated to the current manufacturing, operational and maintenance technologies of the various ways of transport, especially aeronautics, until 2050. The importance of this sector is due to its strong impact on the global economy, having a growth rate of results of 6.8% in the case of aeronautics and European defense enterprises. Therefore, aircraft developed during this period of time should incorporate a high amount of recyclable components that use preferably natural based resources with low environmental impact, hence meeting or even improving the high level of safety required by this sector, without compromising the comfort of the passengers. With these factors in mind, the main objectives of the DesAir project can be divided into two guide lines:

- Development and characterization of a composite material in a Sandwich panel configuration, with high integration of natural components and ability of recycling.
- Development of an optimized and productive process that allows for the fabrication of the panels described in the first guide line in only one operation, envisioning the

maximization of the productive pace compared to the technologies currently in use in the aerospace context.

Within the scope of the QREN program, ACC participates in the AeroCORK project, led by DynAero Iberica (DAI). This project has the main objective of developing sandwich solutions based on carbon fiber and cork cores for the applications and requirements of small ultralight manufactured by DAI. Also in the QREN project scope, ACC, INEGI and Almadesign joined forces to form the L.i.fe project that with direct collaboration of Embraer developed a new concept of aeronautical interiors and sought to study the use of some materials like cork in these applications. ACC also integrates the FIRE-RESIST project that studies new materials intended for various applications such as aeronautics (this part being led by Airbus) in the perspective of fire resistance, be it flammability, smoke generation or toxicity.

1.5 Previous Work

Over the last few years, great effort has been made in order to prove the viability of applying cork based materials in aeronautical and aerospace applications as core materials in sandwich structures. From the mechanical point of view, various sandwich specimens containing carbon or epoxy faces and different kinds of cork agglomerates were subjected to 3 and 4 point bending tests and the results were compared to the mechanical properties of similar specimens using current material cores (Soares, 2007). The evolutions of the load-displacement curves of different cork agglomerates and sandwiches have also been analyzed (Reis & Silva, A. 2009). The mechanical properties and behavior of NL10 and NL30 cork agglomerates, manufactured by Amorim Cork Composites, have also already been studied when subjected to compression, shear and three point bending in which the test specimens were manufactured by Resin Transfer Molding (RTM) process (Carvalho, 2008).

The viability of the development and implementation of cork as a core of a sandwich composite structure for wind turbines blades has been studied (Costa, 2009), and even though cork agglomerate cores didn't show themselves to be suitable due to the superiority shown by the Nomex[®] cores in the bending tests and the intensity of the wind, the results showed that after the compression tests almost all of the original shape was recovered whereas the Nomex[®] cores presented a damaged structure and absolutely no ability to recover their original shape. The ability of a set of optimized cork agglomerates to withstand dynamic loads from a series of impact tests using carbon-cork sandwich specimens has been evaluated and it was shown that cork agglomerates performance essentially depends on the cork granule size, its density and the bonding procedure used for the cohesion of granulates (Castro & Silva, J.M., 2010). The fact that all of these parameters can be adjusted in function of the final application intended for the sandwich component gives a sense of versatility to the cork agglomerates. The feasibility of using cork composites with improved specific strength and damage tolerant properties for aerospace applications was assessed, by combining the natural damping characteristics of cork with high performance composites, such as sandwich structures with a cork-epoxy agglomerate core or carbon-epoxy laminates with embedded cork granulates (Silva, J.M. & Gamboa, 2011). Results showed that, regardless of the type of application, there is reason to be confident about the use of cork based materials in aerospace components due to their noticeable damage tolerant and high energy absorption properties under different loading scenarios.

From a computational standpoint, structural modelling of aeronautical shell components made of sandwich composites with cork cores was used with the objective of the validation of finite element models (Ricardo, 2009). The author also compared the experimental test data under a three-point bending setup with that predicted by MSC Patran[™] 2008, a commercial FEA software.

In an effort of studying the feasibility of the utilization of natural material in structures, tests were carried out in order to explore the acoustic response and damping properties of sandwich composite beams composed with natural materials like cotton and bamboo and compared them over commonly used traditional sandwich composites, which led to the conclusion that it is possible to create a sandwich beam with superior acoustic performance, without minimal sacrifices in stiffness-to-weight ratios (Sargianis, 2012a). Sargianis et al showed that marrying carbon fiber composites with natural cork in a sandwich structure provides a synergistic effect yielding a noise-free sandwich composite structure without the sacrifice of mechanical performance or weight. Furthermore, the cork-core sandwich composites boast a 250% improvement in damping performance, providing increased durability and lifetime operation (Sargianis, 2012b).

However, even though natural material based sandwich composites are receiving increased attention and usage in application, very little work has been done towards the thermal characterization of cork-core sandwich structures. Thermal conductivity tests and aging tests have been performed (Esteves, 2010) in order to characterize and evaluate the thermo-mechanical behavior of new cork-based materials. The influence of temperature and the presence of resin, or lack thereof, on the variation of the mass of cork of two sandwich panels type using cork plates, C270 and C270(R), was also shown (Mir, 2012). At 220°C, the loss of mass is bigger in the C270 cork than in the C270(R) cork, which is due to the fact that C270 cork presents a higher percentage of presence of air between the grains. Thus, the presence of resin inside the cork prevents the mass from decreasing considerably. The work of Veras, (Veras, 2013), characterized thermally and acoustically a set of sandwich structure solutions, also fabricated by Amorim Cork Composites, which are to be utilized as floor panels in the rail industry. The results show that changing variables such as the thickness and the core material led to different performances regarding mechanical, acoustical and thermal behavior.

Although the results obtained in the above mentioned studies show that there still exists significant room for improvement in order for the cork agglomerates to be able to compete with the leading materials, the authors agree upon the fact that cork has a very attractive set of features that point to the potential of it being used as the core material of a sandwich structure.

Chapter 2 - Cork and its properties

Cork has attracted the curiosity of man since ancient times when some of its main properties were reckoned and put to use. Being light and non-water absorbent, it was an adequate material for floats. Cork was also used to plug liquid-containing reservoirs due to its compressible and impermeable nature to liquids. The very low thermal conductivity made it a good insulator for shelter against the cold temperatures and its energy-absorbing capacity was also put to practical applications. Looking at how cork is utilized today, one can easily notice that some of these uses have stayed practically unchanged through time. However, and according to Pereira, it was not until the boom of the chemical industry that synthetic polymers have substituted cork in some applications, either totally such as in fishing devices and buoyancy equipment, or to a large extent such as in cold and heat insulation. However, as a sealant for liquid containers, cork has remained in its essence practically unchanged regardless of the automation and technological innovation introduced in the industrial processing. Although the use of plastic stoppers and aluminum screw caps was started by some wine cellars, the natural cork stopper remains unquestionably “the” closure for good quality red wines. Space vehicles or complex structures under vibration and dynamic loads are examples of their high-tech applications (Pereira, 2007).

2.1 Cork Morphology

Cork is a natural closed-cell foam composed by tiny hollow cells of hexagonal prismatic shape arranged in a space-filling structure without intercellular voids (figure 14). In materials science, a cellular material is defined as a material made up of empty cellular elements, either open or closed, with a solid fraction under 30% of the total volume. In materials with closed cells however, these are polyhedral volumes with solid faces that are in contact with the adjacent cells.

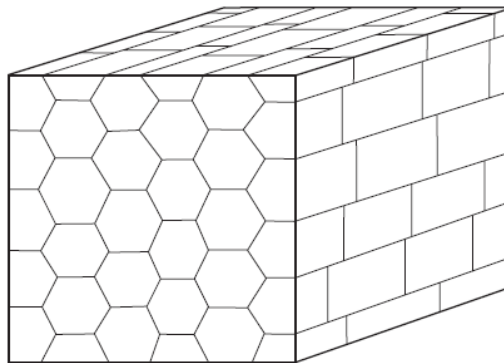


Figure 14 - Diagram of the three-dimensional structure of cork. (Pereira, 2007)

The properties of cellular solids depend on the way the solid is distributed in the cell faces and edges. In such materials, the geometry and dimensions of the cells, as well as their variability, have an important role as well as the three-dimensional arrangement of the individual cells. Cork has a regular structure of closed cells that derive from the one-cell layer of phellogen and grow uni-directionally outwards in the tree's radial direction (figure 15). There are periodic variations in cell size and density resulting from the physiological rhythm of the tree that lead to the formation of growth rings. The regularity of the cellular arrangement is also disturbed by the occurrence of discontinuities, either of biological origin, such as the lenticular channels and woody inclusions, or accidental, such as cracks.

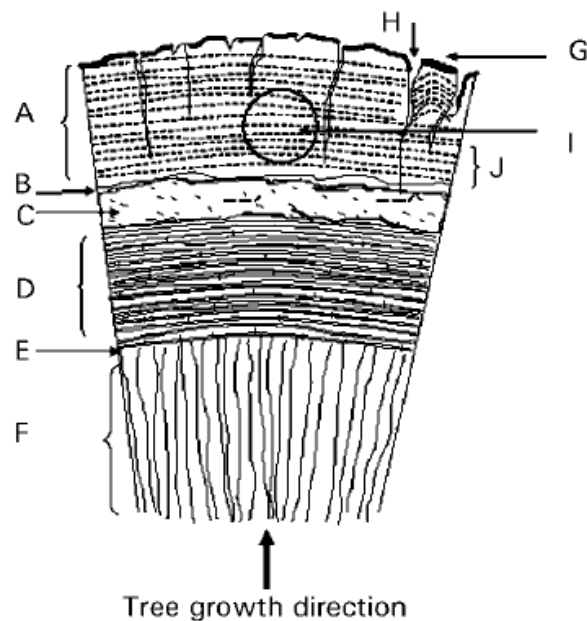
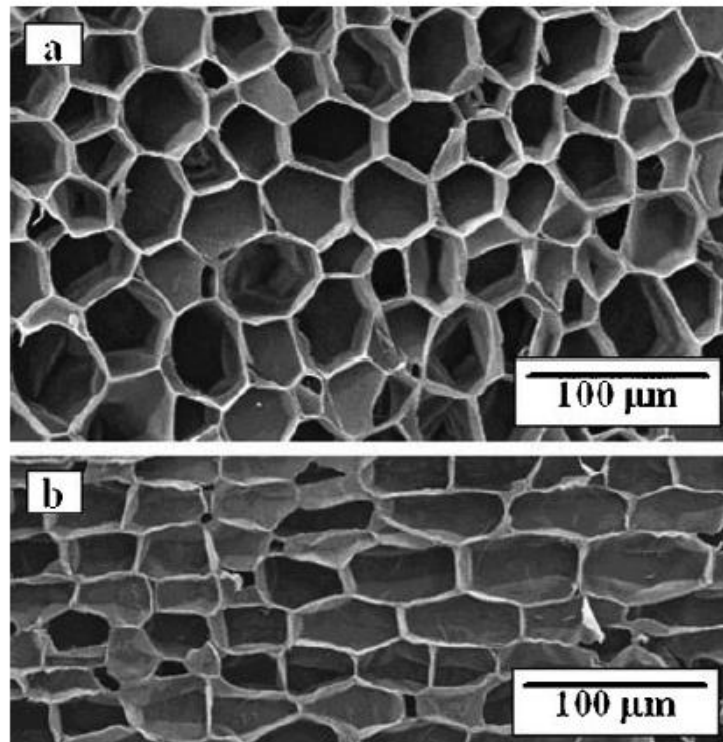


Figure 15 - Schematic representation of axial section of cork oak tree; (A) cork (suberose tissue), (B) subero-phellogenic change, (C) phellogenium, (D) liber tissue, (E) liberwood change, (F) wood, (G) bark, (H) lenticular channels, (I) area for stopper production, (J) annual growth rings (Silva, S.P. & Sabino, 2005)

Cork has an alveolar cellular structure similar to that of a honeycomb and the solid that builds up the polyhedral faces is a natural composite of several biosynthesized polymers (suberin, lignin, cellulose and hemicelluloses). The cellular membranes have a certain degree of impermeability and are full of a gas, usually considered similar to air, occupying nearly 90% of its volume (Gil, 1998). Castro and Silva report that this cellular configuration has a strong influence on the mechanical properties of cork-based materials (Castro & Silva, J.M., 2010).



a radial section; *b* tangential section

Figure 16 - Micrograph of natural cork (after boiling) obtained through SEM (Silva, S.P. & Sabino, 2005)

Table 1 shows a compilation of the main mechanical properties of natural cork obtained from different experimental tests, previously presented in Silva's work (Silva, S.P. & Sabino, 2005). When cork is compressed, its cells become curved and bent, without practically any lateral expansion, with a subsequent recovery taking place given the compressed gas activity found in the cells' interior. More specifically, when cork is compressed in the radial direction, the cell walls fold and pack due to the corrugations, the amplitude of corrugations increases and the cell bases perpendicular to the R direction align. Both these effects cause a small expansion in the NR direction, which results in a small positive value for the poisson coefficient (ν). When the compression is in the NR direction, the lateral cell walls bend, straighten and, at high strains, invert the undulation pattern, which leads to shrinkage in the R direction and hence to a negative Poisson ratio at high strains. Cork is a material that disperses deformation energy. It has an average density of around 200 kg/m³, and a low thermal conductivity. Cork is also of a notable chemical and biological stability and is a good fire resistant material. Macroscopically, cork is a light, elastic material, practically impermeable to liquids and gases, a thermal and electrical insulating material and acoustic and vibration absorber, being also innocuous and practically incorruptible, providing a compression capacity with practically no lateral expansion (Gil, 1998).

Table 1 - General mechanical properties of cork (Silva, S.P. & Sabino, 2005)

Property	Value	Ref.
Compressive modulus, natural cork, unboiled, MPa	8-20 (R)	105, 107, 111
	13-15 (NR)	107
Compressive modulus, boiled, MPa	6 (R)	107
	8-9 (NR)	107
Compressive modulus, heat treated at 100°C, 28 days, MPa	11 (R)	105
	11 (NR)	105
Compressive modulus, heat treated at 150°C, 28 days, MPa	15 (R)	105
	14 (NR)	105
Tensile modulus, boiled, MPa	38 (R)	97
	24-26 (NR)	97
Collapse (buckling) stress, boiled, MPa	0.75-0.8 (R)	24, 111
	0.6-0.7 (NR)	24, 111
Collapse (buckling) strain, %	4 (R)	24
	6 (NR)	24
Fracture stress under tension, MPa	1.0 (R)	24
	1.1 (NR)	24
Fracture strain under tension, %	5 (R)	24
	9 (NR)	24
Fracture toughness, boiled, MPa m ^{1/2}	60-130	97
Poisson's ratio, boiled	0.0-0.097 (V _R /N _R)	24, 100
	0.0-0.064 (V _{NR} /R)	24, 100
	0.26-0.5 (V _{NR} /NR)	24, 100
Loss coefficient at 0.01 Hz	0.1-0.3	24, 78

R, measured in radial direction; NR, measured in non-radial directions.

The characteristics of cork insulation are due to the fact that both gas content and cell size account for the very poor heat transfer properties of cork. Cork cells are much smaller than the cells of other common materials, which helps justify its exceptional insulating properties. Heat can be transmitted by conduction, which depends on the amount of solid in the structure and is less for expanded cork for thermal insulation; convection, which is significant only for high volumes of gas and therefore does not contribute much; and radiation, which becomes less efficient with decrease in cell size. The smaller the size (as is the case of cork), the greater the number of times heat has to be absorbed and re-irradiated (Gil, 1998). Hence, in cork only conduction has importance for heat transfer. The thermal conductivity of the walls will be only slightly higher than that of the gas in the cells (Gil, 2005).

2.2 Ecological and economic importance

Cork is a natural product obtained from the cork oak (*Quercus suber* L.), which is an evergreen oak that is characterized by the presence of a conspicuous thick and furrowed bark with a continuous layer of cork in its outer part. It is this cork bark that gave the cork oak its notoriety and economic importance as a cork producer, as well as its ornamental value in many parks and urban areas around the world. The recognition of the important role of cork oaks in the ecologically fragile regions of southern Europe and northern Africa, where this oak species mostly integrates multifunctional agro-forestry systems, called “montado” in Portugal and “dehesa” in Spain, as a buffer to soil erosion and desertification drew the attention of present environmentalists and researchers (Pereira, 2007). Cork may be stripped off from the stem without endangering the tree vitality and the tree subsequently rebuilds a new cork layer. This is the basis for the sustainable production of cork during the cork oak’s long lifetime. The European Union is the largest cork producer, with over 80%, namely in the Southern Mediterranean countries, of which Portugal distinguishes itself, with over 50% (Gil, 2009) (Pereira, 2012). The cork oak forests are extremely well-adapted to the semi-arid regions of southern Europe, preventing desertification and providing the perfect habitat for many animal and plant species (Gil, 2007).

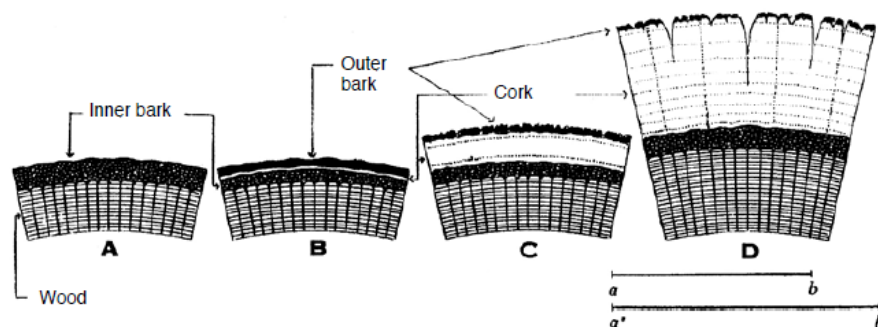


Figure 17 - The growth process of cork (Gil, 2007)

Additionally as the world seeks environmentally friendly materials, the harvesting of cork is a natural, renewable process which reduces subsequent carbon footprints. Regarding the production of expanded agglomerated cork, Gil reports that its manufacturing process only employs superheated steam resorting to boilers fueled by granules obtained from byproducts, amongst others, without making use of any non-cork products (Gil, 2007). Agglomeration also takes place by means of cork’s own resin, resulting in a product that is 100% ecological and natural which constitutes an advantage very difficult to equal by rival materials. In the manufacturing processes of cork building products an important byproduct is produced - cork powder. This powder is currently burnt for the production of steam and/or energy used in the factories themselves or even granted to the electrical network, due to its high energy content.

Therefore, there is no cork byproduct that is not re-used or otherwise valued/ employed. The fact that cork products are thus used is also very important from an ecological point of view because cork is a renewable product of long duration, promoting CO₂ fixation. Furthermore, a cork oak tree that is harvested periodically, will produce between 250% and 400% more cork than what it would produce had it not been harvested, thus developing a higher CO₂ fixation (Gil, 1998).

Sargianis states in his work that a transition from synthetic foam cores to natural cork cores could provide unprecedented improvements in acoustic and vibrational performance in applications such as aircraft cabins or wind turbine blades (Sargianis, 2012b). Given that cork oak trees can take up to 30 years to become productive, reduction in cork's economic viability can lead to insufficient investments in the cork forests. Saving the cork oak, increasing the forest areas, as well as the quantity and quality of cork produced and developing new products, of greater added value, are all fundamental aspects. An important economic loss in the activities of the cork industry, would lead to an uncertain future for the cork forests, promoting losses in biodiversity, land desertification, social imbalance and the disappearance of one of the most sustainable industries (Gil, 2007).

The cork that is produced feeds an important industrial sector that exports its products all over the world. Despite their distinctive characteristics and diverse applications, cork and the cork oak have not been systematically researched until the late 1990s. The fact that the cork oak supports a socioeconomic chain in regions where other crops and activities are scarce also enhanced the recent scrutiny that already allowed recognizing the complexity of the present cork oak agro-forestry systems. The overall sustainability of the cork oak lands as well as the economic soundness of what is the most important non-wood forest product of Europe are key issues. The investigation of properties of cork from a materials science point of view started in the 1980s and studies on the chemical composition of cork enhanced. Important findings on the chemical elucidation of its structural components were obtained since the late 1990s. However, many uncertainties and gaps of knowledge still remain both on the functioning of the cork oak in relation to cork formation and on the understanding of the fundamentals of cork properties. The structural and chemical features of cork are not fully exploited and the present applications do not cover the many possibilities offered by the special properties of this natural cellular material (Pereira, 2007).

2.3 Cork Agglomerates

Agglomerating is the activity which consists of agglutinating granulates, which are made by grinding scraps, parings, virgin cork, cork pieces or stopper production and further used to reduce weight, and other kinds of inferior quality cork which, through the application of heat and pressure in autoclaves, involving steam from superheated water, gives rise to agglomerates (Mestre, A. & Gil. L, 2011). Gil reports that the first agglomerated cork stoppers were developed in the beginning of the XX century using several types of glues, some of the being dextrin, casein, gelatin, urea-formaldehyde and amine, and in 1968 polyurethane was used (Gil, 2000). In the market there are several types of cork agglomerates, which the author divides into two categories: composition cork and insulation corkboard. Given that the latter is made exclusively of cork without any external binding agents or any other added material, it cannot be considered as a true composite material.

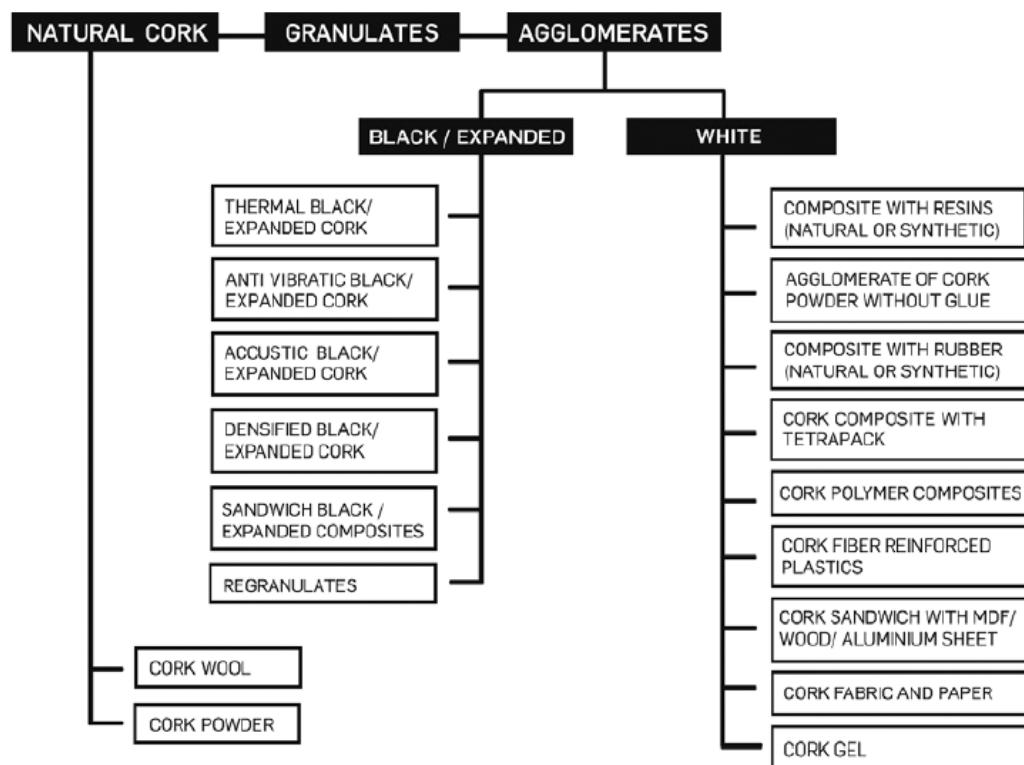


Figure 18 - Cork Agglomerates Types (Mestre, A. & Gil. L, 2011)

Composition cork on the other hand is made of granules which have been joined together using different synthetic or natural binding agents, such as urethane, melaminic and phenolic resins, yielding products such as agglomerated cork stoppers, floor coverings, joints, etc. The physical and chemical characteristics of the binders determine the strength of agglomerate and therefore its applications (Gil & Silva, 2000).

Chapter 3 - Experimental Characterization

In this chapter, the fabrication of the samples is discussed as well as the experimental setup used in the thermal tests. These experimental tests are carried out in order to thermally characterize the cork core sandwich panels. Computer Numerical Controlling, or CNC, equipment was used for the manufacture of the cork cores while the aluminum face sheets were cut using a hole saw. The internal diameter of the hole saw matches the diameter of the numerical models. All the tools that were used for the manufacture of the samples, including the CNC machine and the hole saw, were provided by University of Beira Interior.

3.1 Manufacture of the test samples

The first objective is to properly cut and extract the circular face sheets from a set of 300 mm by 300 mm, 1 mm thick, square aluminum sheets (Aalco 5754) using a bi-metal hole saw with an 152 mm external diameter, depicted in figure 19 and figure 20 respectively. This had to be done before cutting the cork agglomerate cores, due to the non-adjustable nature of the diameter of the hole saw and although the diameter of the hole saw is 152 mm, the cut diameter has a different value. Since that the teeth of the hole saw have a thickness of about 2 mm, the final cut diameter was expected to be 148 mm. These aluminum face sheets, as well as the NL20 cork agglomerate plates, were provided by Amorim Cork Composites.



Figure 19 - Aalco 5754 square aluminum face sheets



Figure 20 - Bi-metal 152 mm hole saw

Although the hole saw is designed to cut through metals such as aluminum, care had to be taken during the cutting process. The rotation speed had to be adjusted in order to maintain the aluminum's temperature at an acceptable level and avoid damaging the hole saw's teeth. The aluminum sheets had been previously cut by Amorim Cork Composites in 300 mm by 300 mm

square sheets with the objective of extracting exactly four circular face sheets with minimum aluminum waste.

Given that there are nine different circular sandwich models, there would have to be at least eighteen circular aluminum face sheets (a frontside face sheets and a backside face sheet), which does not include the spare samples or replicas of each model. The hole saw was attached to a milling machine, illustrated in figure 21, to ensure that the angle between it and the aluminum face sheet was as close to 90° as possible. When the hole saw, which could only be moved in the vertical direction and was already rotating at a lower speed rate, touched the face sheet, the handle had to be carefully pushed down in order to cut progressively through the aluminum sheet. Figure 22 shows the complete experimental setup, which besides the milling machine and the hole saw, is comprised by a set of clamps which hold the aluminum face sheet firmly against the wooden sacrificial board.



Figure 21 - Milling machine with hole saw



Figure 22 - Cutting process of the aluminum sheet

The extracted aluminum face sheets, illustrated in figure 23, presented a diameter of about 147 mm. Therefore, the first objective was completed. The second objective is to extract nine circular samples from a 1000 mm by 500 mm plate, with a thickness of 18 mm, made of the NL20 cork agglomerate fabricated and provided by Amorim Cork Composites (see figure 24). In addition to the circular profile cut, there was also a set of different drilling patterns to be made on the cork plate, both of which are done by the CNC machine.



Figure 23 - Extracted Aluminum face sheet



Figure 24 - Original NL20 Cork agglomerate plate

It is worth noting that the drilling patterns and the dimension values of the samples were designed in CATIA V5®, after calibrating the hole diameters and distances between holes in ABAQUS® to ensure that the samples had the desired mass values. This had to be done by trial and error since there is now mass configuration tool. Figure 25 shows a preview of the finished plate, with the cork samples already cut in circular profiles.

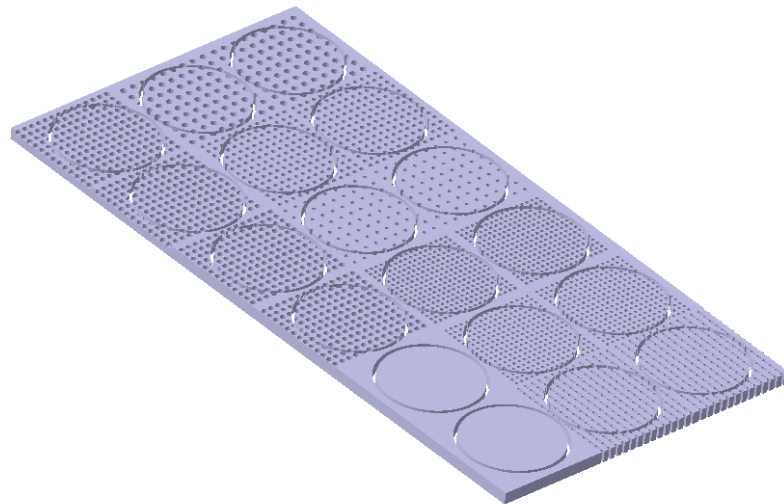


Figure 25 - Preview of the cork plate with drilling patterns developed in CATIA®

The complete model had to be saved in a drawing with a .dxf format containing the top and the bottom views so that it could be imported to the 2D and 3D component modelling program Aspire®. This program works with data codes containing the coordinates and references of the cork plate, as well as the type of operation to be performed by the CNC machine, also known as toolpaths which are necessary to accurately cut the desired shapes. In the present thesis, these files are integrated in .tap extension files, which are compatible and transferred to the CNC machine via a USB pen drive. Once the reference origin in the x, y and z directions of the machine had been set in accordance with the toolpath files, the job was ready to run on the CNC machine (see figure 26).

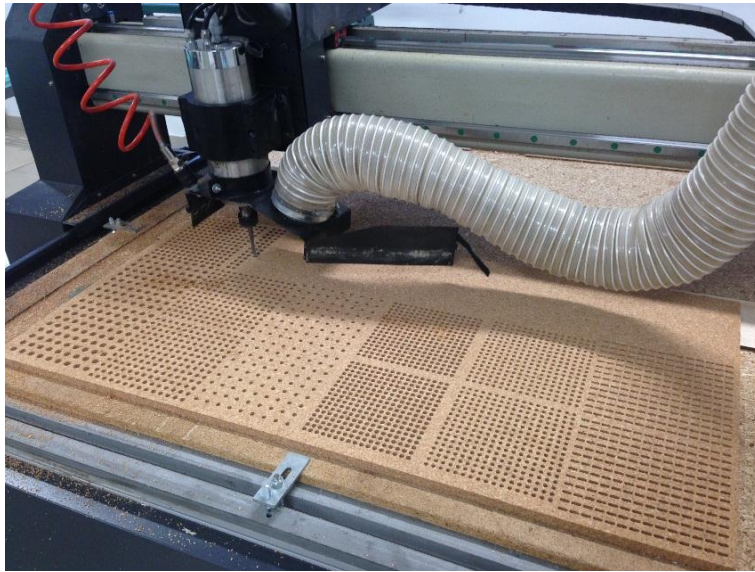


Figure 26 - Development of the drilling patterns

Standard end mills with different diameters ranging from 4 mm to 10 mm were used to drill the holes. Taking into account that not all of the drilling patterns were based on through holes, the plate had to be flipped without changing the initial reference point in order to drill holes with 6 mm depth on the other side of the non-through hole patterns. This was achieved by the use of two wooden corners attached to the sacrificial board (at the upper left and right corners in figure 27), which mark the exact position of the plate. Before the drilling process began, the plate was attached to the sacrificial board via adhesive tape. A standard end mill with a diameter of 5 mm was used to cut the outer circular profile of the samples since that a smaller diameter could lead to a damaged mill.

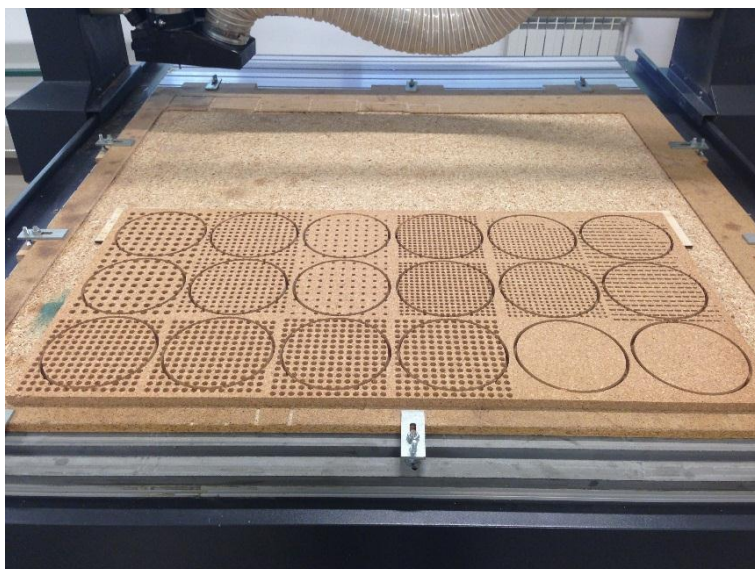


Figure 27 - Finished Cork Plate with drilling patterns and profile cuts

Figure 27 shows the finished plate already flipped which means that the separated cork samples are ready to be extracted. Looking closer at the upper right corner of the plate, it seems that some holes are missing, but it is really an ultra-thin cork peel (smaller than 1 mm) which can be easily removed with a sharp object. Looking at the rendered image of the Cork plate designed in CATIA® in figure 28, and comparing it to figure 27, there are no discrepancies whatsoever.

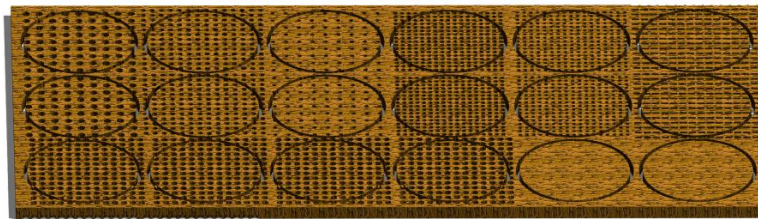


Figure 28 - Rendering of the finished cork plate designed in CATIA®

It was previously established that the CNC machine left three small cork tabs around each cork sample with a 120° circular spacing so that there would be no movement or slippage during the profile cut (see figure 29).



Figure 29 - Small tab that prevents any movement by the cork sample

After cutting the tabs, the remaining cork parts were carefully removed to avoid causing any damage to the samples. The final product is illustrated in figure 30.

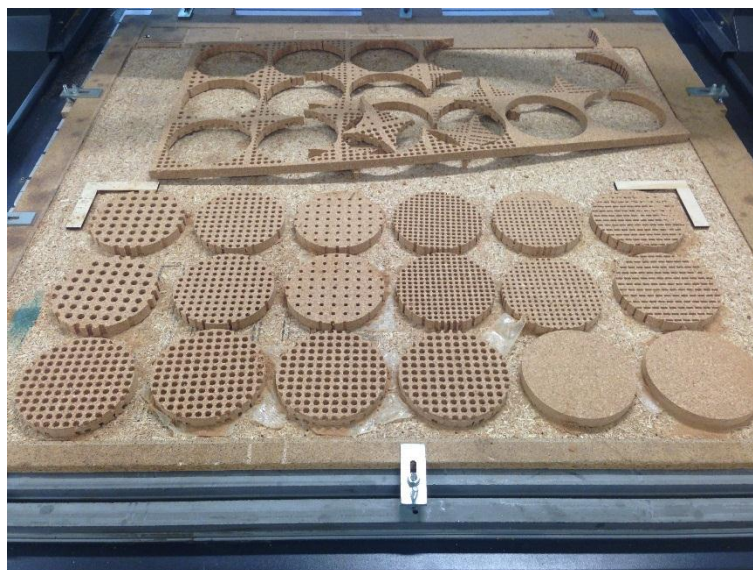


Figure 30 - Extracted Cork Samples

After being successfully extracted, each cork sample had to be individually weighed. Table 2 shows the final weight of every samples compared to the expected weight given by ABAQUS®. A relative mass error between the real weight and the expected weight is calculated and given by:

$$\varepsilon_{mass} = \frac{W_{real} - W_{expected}}{W_{real}} \quad (3.1)$$

Table 2 - Weight and expected weight values for the core samples

Model description	Weight [g]	Expected Weight [g]	Error [%]
Uniform	65.98	63.6	3.607
Bracket pattern	48.49	46.8	3.485
5.14 mm	47.95	46.9	2.190
6 mm (a)	40.31	40.0	0.769
6 mm (b)	59.24	57.5	2.937
7 mm	48.70	46.9	3.696
Non-through (a)	49.21	46.9	4.694
Non-through (b)	48.66	46.8	3.822
10 mm	48.75	46.9	3.795

The non-through hole models present two of the more significant mass differences while the lighter 6 mm through hole model practically weighs as expected. The average error is of 3.222% which corresponds to a weight difference between 1 and 2 grams, depending on the model. The aluminum face sheets have also been weighed and assigned to each model with a “top” or “bottom” description, which corresponds to the frontside and the backside, respectively. The expected weight value is the same for each face sheet, whether it is a top or a bottom sample.

Table 3 - Weight and expected weight values for the top and bottom face sheets

Model description	Relative Position	Weight [g]	Expected Weight [g]	Error [%]
Uniform	Top	44,50	45.80	2,838
	Bottom	44.53	45.80	2.773
Bracket pattern	Top	45.24	45.80	1.223
	Bottom	44.89	45.80	1.987
5.14 mm	Top	44.16	45.80	3.581
	Bottom	43.96	45.80	4.017
6 mm (a)	Top	44.88	45.80	2.009
	Bottom	45.15	45.80	1.419
6 mm (b)	Top	44.25	45.80	3.384
	Bottom	44.50	45.80	2.838
7 mm	Top	44.65	45.80	2.511
	Bottom	44.17	45.80	3.559
Non-through (a)	Top	45.47	45.80	0.721
	Bottom	44.50	45.80	2.838
Non-through (b)	Top	45.37	45.80	0.939
	Bottom	45.07	45.80	1.594
10 mm	Top	44.58	45.80	2.664
	Bottom	45.27	45.80	1.157

Similarly to the core samples, a relative mass error was calculated for the face sheets using equation 3.1. In this case, the average error equals 2.336%, which is slightly less than that of the core samples. Now that the core samples and the face sheets had been fabricated, they had to be joined together. A glue mixture made of SikaForce® 7710 L-100 (component A) and SikaForce® 7010 (component B) was used to make the aluminum adhere to the cork samples (see Figure 31). A ratio of 100 grams to 19 grams was used between component A and component B, respectively.



Figure 31 - Glue componentes (A and B)

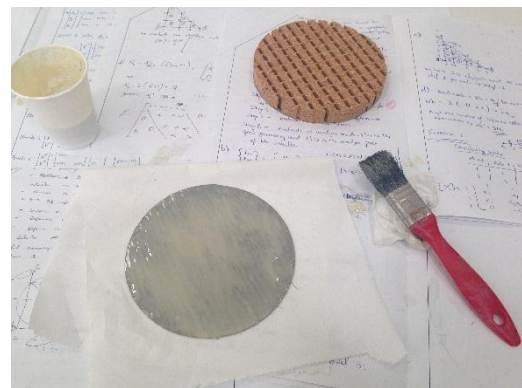


Figure 32 - Application of the glue mixture

After obtaining a homogeneous mixture, the inner side of each face sheet was applied with glue using a regular brush and the outer side was marked with the corresponding model description (see Figure 32). Although the core sample is included in figure 32, no glue mixture was applied to it. The joined assembly went through a twenty four hour curing process with

heavy weights such as batteries on top to ensure the quality of its integrity. Figure 33 shows all assemblies after the curing process.



Figure 33 - Final assemblies after curing process

Although the assemblies were completed, the edges around the face sheets had to be smoothed over with sandpaper in order to avoid cuts and to exactly match the face sheet diameter to the core diameter. Figure 34 and figure 35 show the top face sheet edge of the heavy version of the 6 mm through hole model before and after the smoothing, respectively.

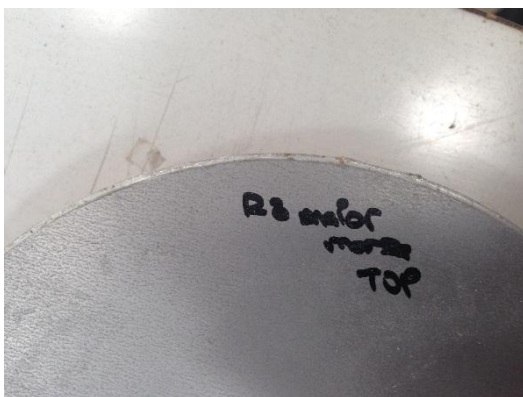


Figure 34 - Top face sheet edge before smoothing

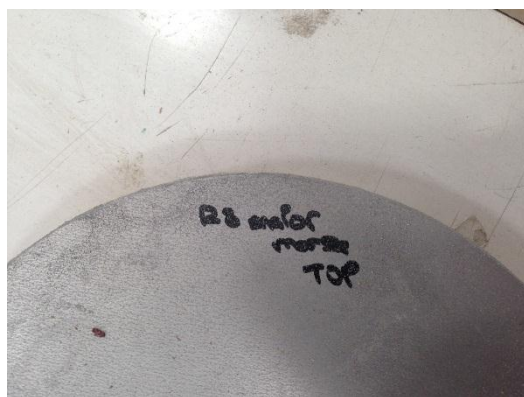


Figure 35 - Top face sheet edge after smoothing

Next up the top and bottom face sheets had to be cleaned in order to avoid compromising the uniformity of the temperature distribution on the face sheet which could affect the quality of the experimental results. Once cleaned, the samples were weighed one more time to evaluate the effect of the glue on the final weight. Table 4 shows the weight after the curing process compared to the combined weight of the face sheets and the core samples before being joined.

Table 4 - Final assembly weight compared to the combined weight of the individual parts

Model description	Weight After [g]	Weight Before [g]	Error [%]
Uniform	165,64	155,01	6,418
Bracket pattern	153,49	138,62	9,688
5.14 mm	145,38	136,07	6,404
6 mm (a)	138,49	130,34	5,885
6 mm (b)	158,73	147,99	6,766
7 mm	148,14	137,52	7,169
Non-through (a)	150,91	139,18	7,773
Non-through (b)	148,29	139,10	6,197
10 mm	148,65	138,60	6,761

The error values of the table above lead to the conclusion that the glue mixture present in each assembly has some influence on the final weight of the assembly given that the average error is of 7,007%, which equals between 10 grams and 11 grams, depending on the model. A similar analysis was carried out between the weight of the assembly after the curing process and the expected weight of the assembly calculated in ABAQUS®.

Table 5 - Final assembly weight compared to the expected weight from the numerical analysis

Model description	Weight [g]	Expected Weight [g]	Error [%]
Uniform	165,64	155,20	6,303
Bracket pattern	153,49	138,40	9,831
5.14 mm	145,38	138,50	4,732
6 mm (a)	138,49	131,60	4,975
6 mm (b)	158,73	149,10	6,067
7 mm	148,14	138,50	6,507
Non-through (a)	150,91	138,50	8,223
Non-through (b)	148,29	138,40	6,669
10 mm	148,65	138,50	6,828

The fact that in this case the average error is of 6,682%, which is close to the previous average error of 7,007%, shows that there is little difference between the expected weight from the numerical analysis and the combined actual weight of the individual parts before being joined, in other words, without the glue mixture. This conclusion can also be drawn by analyzing and comparing the “Weight Before” values and the “Expected Weight” values from table 4 and table 5, respectively. Although the assemblies were finished, they were not yet ready to be tested since that there was no thermal insulation on the sides. Therefore, Sika Boom®-S, a one part polyurethane expansive insulating adapter foam, illustrated in figure 37, with a service temperature up to 100°C was used to insulate the sides of the assemblies.

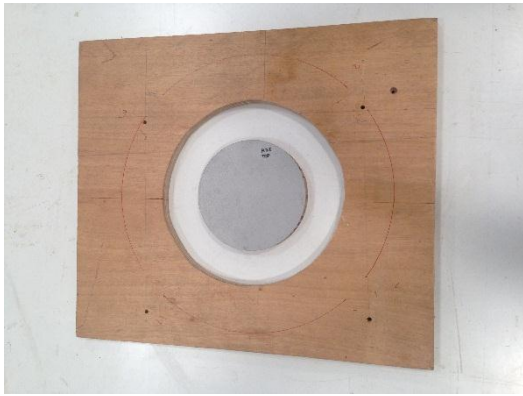


Figure 36 - Fully expanded polyurethane foam



Figure 37 - First mold version (without cover)

Although polyurethane foam is not a perfect insulator, it has a powerful thermal insulating ability and about the same thermal conductivity as cork, which is of 0.04 W/m.K (Sika, 2007). Seeing that this polyurethane foam needs some time (up to 24 hours) to fully cure, a mold for each test sample had to be constructed so that the foam would take the desired shape without overflowing to the outer faces of the face sheets. The first version of the mold, in figure 36, had no cover which led to a bigger expansion and consequently lower density of the insulation foam, which can be seen in figure 37. In order to increase the density and the precision of the shape, a new mold closed by a cover was constructed in which the foam would enter through a hole on the side (see Figure 38 and Figure 39). The new mold has a smaller diameter, relatively to the first version, which means that while the new version has a more dense lateral insulation, the first version has a thicker tear of insulating polyurethane foam.



Figure 38 - New molds with holes (open)



Figure 39 - New mold with cover and clamps (closed)

Another hole was made on the opposite side so that the foam could exit through it which determined if the mold had enough foam on the inside, as illustrated in figure 39. The cover had a plastic foil on the inner side so that the foam would not stick to it and consequently preventing it from being removed afterwards. Figure 40 shows four of the new molds with covers on which pressure is applied by the clamps. After a 24 hour curing process, the foam is visibly fully expanded as it came out both holes and dried up.



Figure 40 - Closed molds with fully expanded foam

After cutting the excess of foam that came out the holes, the covers were carefully removed in order to avoid damaging the foam. The circular tear of foam had dried up successfully and presented the desired shape, as depicted in figure 41. Care had to be taken to cut and extract all of the test samples from their molds. After cutting the little excess of foam present on the top face sheet of some models, all of the nine test samples were ready to be tested (see figure 42).

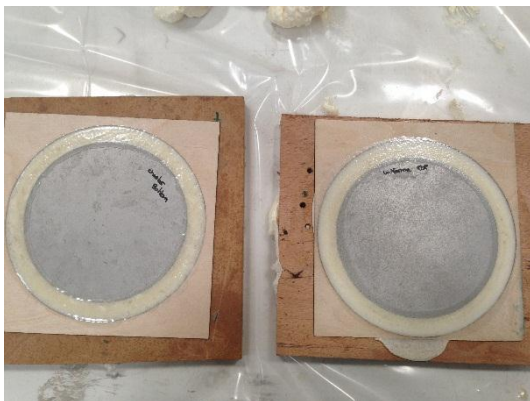


Figure 41 - Test samples after removing the mold cover



Figure 42 - Finished laterally insulated test samples

3.2 Experimental Setup

The test samples were placed all at once on a rectangular heating plate (see figure 43). This ensures that they are all submitted to the same conditions at the same time. The temperature of the heating plate is controlled by an alternating current transformer, also known as autotransformer, shown in figure 44. The test samples were heated by increasing the temperature progressively and at a very slow pace in order to avoid damaging the heating plate. This also means that the test samples will be in a state of equilibrium, or steady state condition, shortly after the plate reaches its desired temperature, given that the transition was made in that fashion. The desired temperature is 80°C due to limitations of the heating plate's service temperature.



Figure 43 - Test samples placed on heating plate



Figure 44 - Alternating current transformer

Attached to the heating plate is a type T thermocouple made of copper and copper-nickel, with a temperature range from -250°C to 350°C and a standard error of 1.0°C or 0.75% (whichever is greater) above 0°C, or 1.0°C or 1.5% below 0°C. This thermocouple indicates the temperature of the heating plate at each instant. The contact thermocouple, illustrated in figure 45, directly measures the temperature of any object it comes in contact with, which in this case will be the test samples. The upper temperature is the one from the thermocouple which is fixed on the heating plate, thus indicating its temperature with a slight error, and the lower temperature is the one given by the contact thermocouple. Directly above the heating plate stands a thermographic camera, also known as infrared camera or thermal imaging camera, which besides indicating the temperature distribution of the environment it scans, gives a temperature range through color correspondence. Figure 46 shows the thermographic camera

pointed down. The camera was positioned so that it could capture the entire heating plate and all of the test samples from above at once.



Figure 45 - Contact thermocouple



Figure 46 - Thermographic camera placed directly above the test samples

The data input sent from the thermographic camera is read by the infrared thermal imaging system Thermo Tracer TH1100 (San-ei Inc.), illustrated in figure 47. The temperature resolution is 0.1°C and the frame time for one image is 1 second. The thermal tests would be carried out with the lights off so that there would be minimum interference with the infrared camera, even though it would not be significant due to the high temperature values.

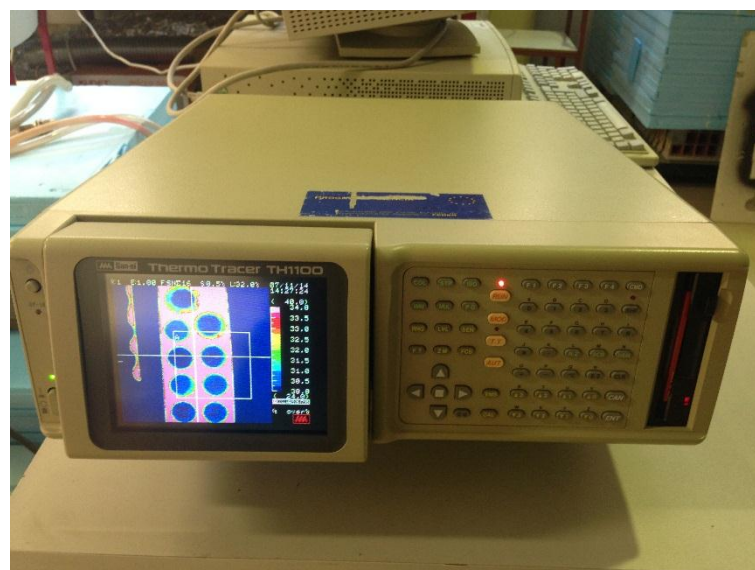


Figure 47 - Infrared thermal imaging system Thermo Tracer TH1100

Figure 48 shows the complete experimental setup, comprised by the heating plate, the test samples, the auto transformer, the thermographic camera, the infrared thermal imaging system and the contact thermocouple along with the fixed thermocouple.



Figure 48 - Complete experimental setup

In chapter 5, the experimental results will be shown along with the experimental determination of the convective heat transfer coefficient. Only after knowing the real convective heat transfer coefficient, or film coefficient, the thermal numerical analysis can be carried out in order to obtain the theoretical results and compare them to the experimental results.

Chapter 4 - Numerical modeling of Sandwich Panels

In this chapter a description of a set of numerical models is given along with the explanation of the numerical analysis to be performed. The numerical models and their respective simulations were carried out using the finite element method code ABAQUS® v6.10-1. These models consist in circular sandwich panels with different drilling patterns in their core. The face sheets however have no holes or drilling patterns. The sandwich panels have their circular form due to the fact that otherwise it would not be possible to avoid the boundary effects which are predominant in the corners where the heat flow is strongly three dimensional whereas in the central area the heat flow is approximately two dimensional (Beausoleil-Morrison, 1995). This results in a bigger heat loss which ultimately leads to an irregular temperature distribution on the downstream face sheet. Thus, in the circular panels the heat loss is the same at any point of the edge. In order to ensure one-dimensional heat-flow, the sandwich panels are laterally insulated. Therefore, the only heat loss that occurs is through convection between the surrounding air and the downstream face sheet. It is important to mention that in order to simplify the analysis, heat loss through radiation can be neglected since it has very little influence on the results, as will be demonstrated below.

4.1 Numerical model description

In the view of the aforementioned morphology concepts, a circular sandwich core is considered with a diameter of 147 mm and a thickness of 18 mm. It is worth noting that in order to be more sensitive to the dimension and mass values, these will be expressed through millimeters and grams, which integrate a sub-division of the international system. The material elected for this part is the NL20 CoreCork® agglomerate developed by Amorim Cork Composites. According to ACC's CoreCork datasheet (Amorim Cork Composites, 2009), this core material has a density of 200 kg/m³ and a thermal conductivity of 0.044 W/m.K established by the norms ASTM C271 and ASTM E1530, respectively. These properties are defined to the section of the model as an isotropic material. The face sheets on the other hand are each 1 mm thick with the same diameter as the core material and weigh 45.8 grams. The material established for the face sheets is aluminum, with a density of 2700 kg/m³ (Engineering Toolbox, 2014a) and a thermal conductivity of 215 W/m.K (Engineering Toolbox, 2014b). Just like the core section, these properties are defined to the face sheet section as an isotropic material.

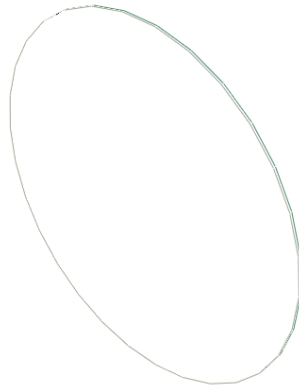


Figure 49 - 1 mm thick aluminum face sheet

The assembly is defined by the cork core material sandwiched between the two aluminum face sheets, with a final thickness of 20 mm. In order to correctly define the contact areas of this model, a constraint of the type “tie” is established between the core faces and the face sheets. The diameter of the assembly has its value due to the outer diameter of the hole saw that was used to cut the samples for the experimental study.

A total of nine different models are simulated and developed based on deformable solid extrusion features. These models differ in their drilling patterns which include a bracket pattern, various circular through hole patterns and a pair of non-trough hole patterns. There is also the uniform sample (see figure 50), which has no holes or drilling patterns. For obvious reasons, this is the heaviest model, with 63.6 grams. The thermal insulation performance of this model is compared to the performances of the remaining models in order to investigate the effect that the introduction of holes has on the overall insulation ability of the sandwich panel. Other than this model and a pair of 6 mm hole models, all other models have the same mass of 46.9 grams. There is however an error of 0.1 grams, which means that while some weigh 46.9 grams, other models weigh 46.8 grams. Given that this error represents less than 0.5% of the total mass of the core, it is found to be practically negligible.

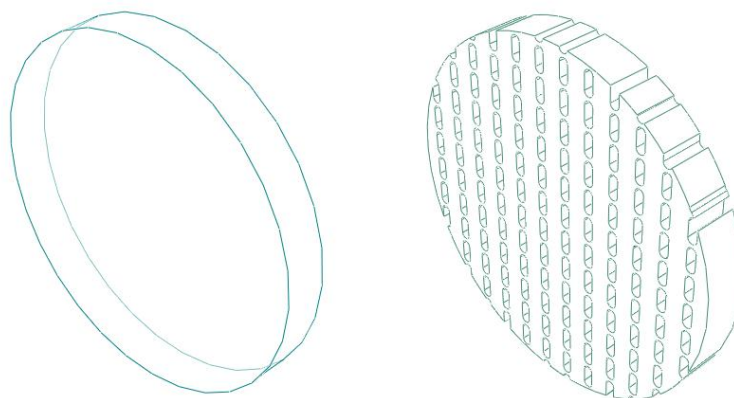


Figure 50 - Cores of the uniform model and the bracket hole model (l. to r.)

The bracket hole pattern has a maximum vertical dimension of 10.52 mm while the maximum horizontal dimension measures approximately 4.01 mm. Each hole has a vertical and horizontal spacing of 12.04 mm, from center point to center point (see figure 50). The purpose of this model is to investigate the influence of the shape of the hole on the overall thermal performance of the sample, by comparing it to the circular hole samples. Finally, the circular hole pattern models comprise 7 different samples, including the two aforementioned non-through hole models and the through hole models with drilling diameters ranging from 5.14 mm to 10 mm. Although the samples below have different hole diameters, which measure 5.14, 7 and 10 mm respectively, the mass was kept constant (see figure 51). The spacing between holes on these models is 8.93 mm, 12 mm and 17.48 mm, respectively.

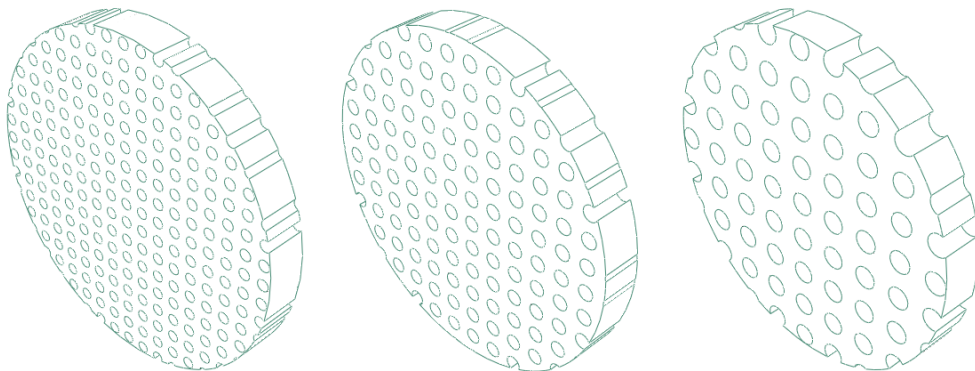


Figure 51 - The 5.14 mm, 7 mm and 10 mm hole models (l. to r.)

Although the main goal of these models resides on investigating the influence of the hole diameter, there are two more objectives within this study. The first one is to explore any discrepancies in thermal isolation performance between through hole and non-through samples. Both non-through models will also be compared to each other in order to explore the effect that the 6 mm offset between the hole patterns of the two faces has on their performance.

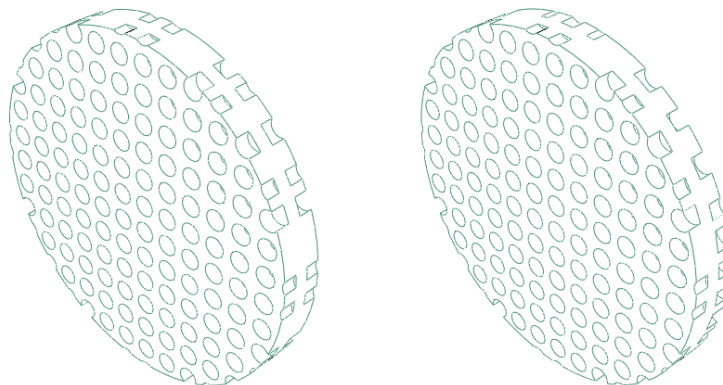


Figure 52 - Non-through hole models without offset and with offset (l. to r.)

These models have the same hole diameter of 8.56 mm, same mass and the same spacing between holes, which measures 12 mm. The thickness of the cores was basically divided in three portions since the holes on both faces have a depth of 6 mm, which leaves a 6 mm thick portion of cork in the middle, as illustrated in figure 52.

The second objective is to study the influence of the mass of cork, or lack thereof, on the overall thermal isolation performance, by comparing two samples with the same hole diameter, which is 6 mm, but different masses (40.0 grams and 57.5 grams), as illustrated in figure 53. This way it is possible to verify if the introduction of air is beneficial to the insulation ability of the sandwich panel. The hole spacing of the heavy model is 17.48 mm while the light model has a 8.74 mm hole spacing which is exactly half of the heavier model, meaning that in this model there is a hole midway between every two holes of the other model.

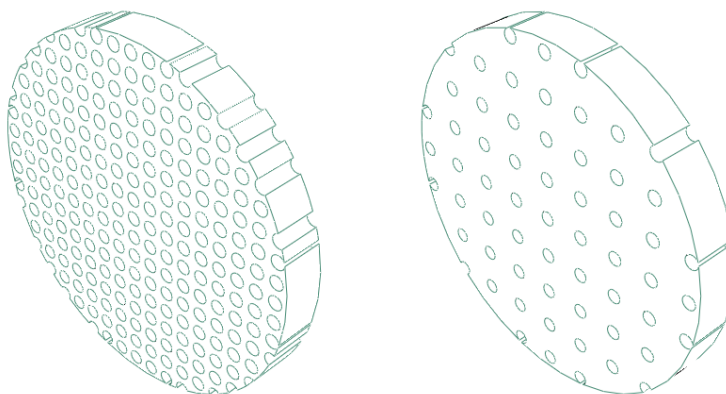


Figure 53 - The 6 mm models intended for the mass study

The following table summarizes some of the information given about the models.

Table 6 - Model description and study purposes

Model description	Hole Shape	Mass [g]	Study purpose	Observation
Uniform	-	63.6	Reference Model	-
Bracket pattern	Bracket	46.8	Hole Shape Influence	-
5.14 mm	Circular	46.9	Hole diameter Influence	-
6 mm (a)	Circular	40.0	Mass Influence	Light
6 mm (b)	Circular	57.5	Mass Influence	Heavy
7 mm	Circular	46.9	Hole diameter influence	-
Non-through (a)	Circular	46.9	Cork presence in holes	8.56 mm/No offset
Non-through (b)	Circular	46.8	Cork presence in holes	8.56 mm/Offset
10 mm	Circular	46.9	Hole diameter influence	-

It is worth noting that no convection was taken into account inside the pockets of air of the holes. Therefore, it is assumed that there is no air movement between the aluminum face sheets. These air pockets are represented by cylindrical solids with the shape of each hole and the thermal conductivity of air (see figure 54 below).

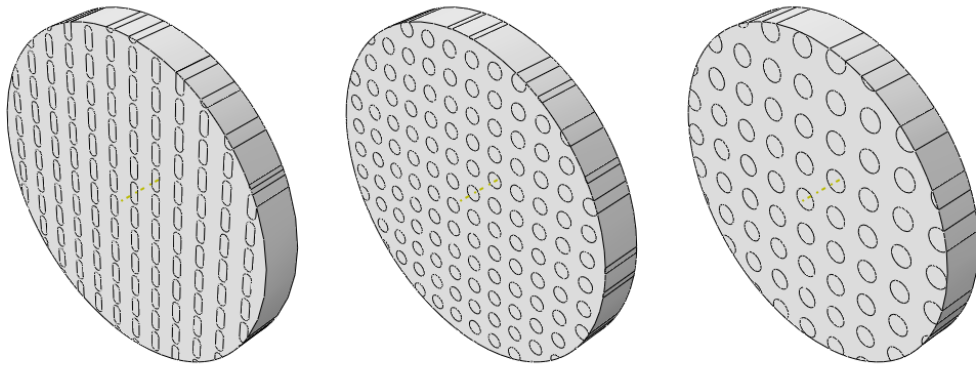


Figure 54 - Isometric view of the completely partitioned models

Thus, the heat is transferred from the cork to the air via conduction instead of convection, which would correspond to the real case. This simplification was done in order to avoid the definition of complex tie conditions between the contact zones of the cork and the air which has a bigger error percentage associated to it and leads to less precise results. After creating a 2D partition on one face via the sketch tool, the partition was projected along the thickness of the model to the opposite face, thus adding an additional dimension to the partition. Once the 3D partitioning of the model was complete, the sections had to be assigned in order to define the properties of each zone. While the previously created partitions were assigned the air section, the remaining partitions were assigned the NL20 cork agglomerate section.

As mentioned earlier, the assembly consists of the core sandwiched between two face sheets. Therefore, it is necessary to define tie conditions in order to properly join these three parts. These conditions are formally known as constrains and to correctly achieve them, the contact zones between the core and the face sheets had to be specified. The contact zones are as highlighted in figure 55.

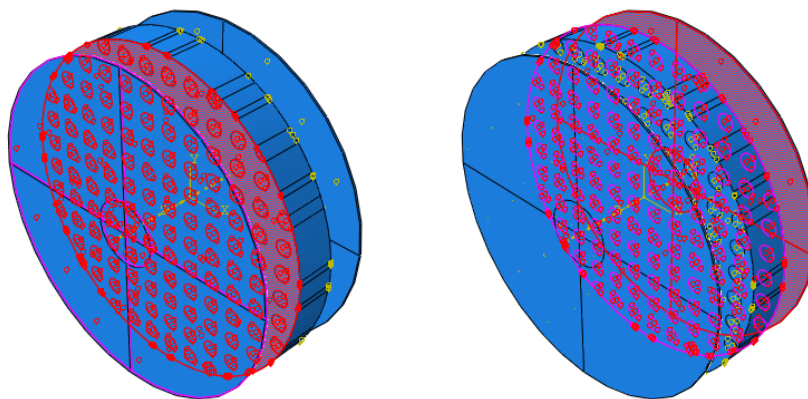


Figure 55 - Frontside and backside tie constrains (l. to r.)

There are two types of boundary conditions applied. The first boundary condition is the heating of the outer face of the backside face sheet, which would elevate the temperature of that zone to 80°C and keep it at that level. The heating temperature has its value due to limitations imposed by the hot plate used in the experimental tests. The zone selected for the backside face sheet heating is highlighted in figure 56.

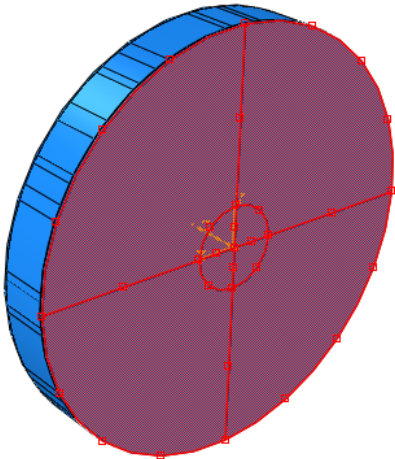


Figure 56 - Highlighted surface for backside face sheet heating

For every surface that has no temperature, heat flux load or interaction type assigned to it, ABAQUS® assumes that there is no heat flux through the surface. Therefore, these surfaces are taken into account as being thermally insulated, which in this case is the whole side of the model, as illustrated in figure 57. This is the second boundary condition. As mentioned earlier, this boundary condition has been applied to the model in order to ensure that the heat transfer through the sandwich panel becomes essentially one dimensional.

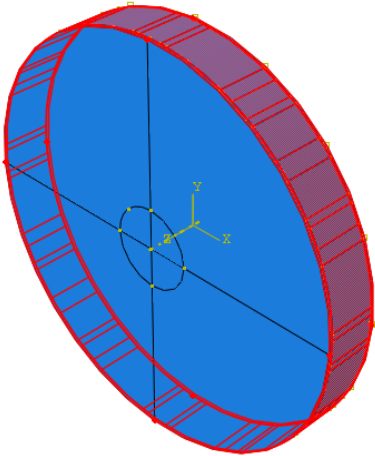


Figure 57 - Selection of the thermally insulated side of the model

In every simulation, a step has to be specified. Therefore, a general heat transfer procedure is chosen for the step. There are two types of heat transfer analysis which are steady state and transient. In steady state conditions the temperature differences and heat fluxes driving the heat transfer remain constant with time, meaning that a state of equilibrium was reached where the spatial distribution of temperature does not change with time. The transient state on the other hand is characterized by variations in body temperature with time. In the present case, a steady state analysis is performed, which means that the heat transfer process has been taking place for a while and an equilibrium state has been reached. The only interaction taking place in this analysis is called *surface film condition*, which consists in convective heat transfer. The sink temperature here is the same as the ambient temperature measured in the experimental tests, which is set at 30°C. The surface elected for this type of interaction is the outer face of the frontside face sheet highlighted in figure 58.

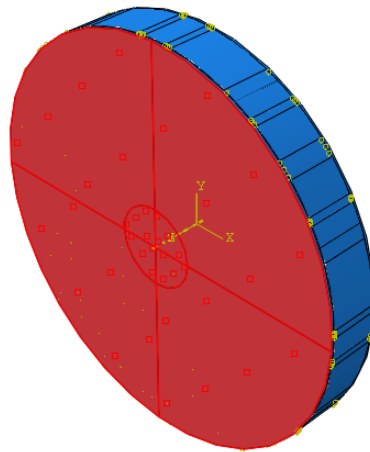


Figure 58 - Highlighted surface for convective heat transfer

For many situations of practical interest, the value of the convective heat transfer coefficient is still known mainly through experiments. Therefore, after the experimental tests were carried out, the real value of the film coefficient was calculated in order to run the numerical simulations again and obtain more accurate results. Given the values of the combined thermal conductivity, the heating temperature, the outer temperature of the frontside face sheet and the temperature of the surrounding environment, it is possible to determine the convective heat transfer coefficient, or film coefficient. In this case, Fourier's law for conductive heat transfer can be used in its one-dimensional form:

$$\frac{\Delta Q}{\Delta t} = -k * A * \frac{\Delta T}{\Delta x} \quad (4.1)$$

Where $\Delta Q/\Delta t$ is the heat flow rate, in Watt, k is the thermal conductivity of the material, in W/m.K, A is the heat transfer area, in m^2 , ΔT represents the temperature difference between

two ends, which in this case are the outer faces of the two face sheets, and Δx is the distance between these ends. On the other hand, the heat transfer through convection can be expressed through Newton's law of cooling, which is a solution of the differential equation given by Fourier's law:

$$\frac{dQ}{dt} = h * A * (T_s - T_\infty) = h * A * \Delta T_s \quad (4.2)$$

Where h is the convective heat transfer coefficient or film coefficient, in $W/m^2.K$, T_s is the temperature of the surface of the object, which in this case is the outer face of the frontside face sheet, and T_∞ is the temperature of the surrounding environment. In both the conductive heat transfer and convective heat transfer, the temperature variables can be expressed in K or $^\circ C$, since these variables are involved in temperature differences, which consist in subtractions.

Taking into account that the tests are carried out in steady state conditions and that a state of equilibrium has been reached, the heat fluxes remain constant with time. Therefore, it can be assumed that the conductive heat transfer flow is equal to that of the convective heat transfer:

$$-k * A * \frac{\Delta T}{\Delta x} = h * A * \Delta T_s \quad (4.3)$$

Since the heat transfer area variable, A , appears on both sides of the equation, this relation can be simplified as:

$$-k * \frac{(T_s - T_1)}{\Delta x} = h * (T_\infty - T_s) \quad (4.4)$$

Where T_1 is the temperature of the outer face of the backside face sheet. In order to further understand the relation shown above, the following situation in figure 59 is considered:

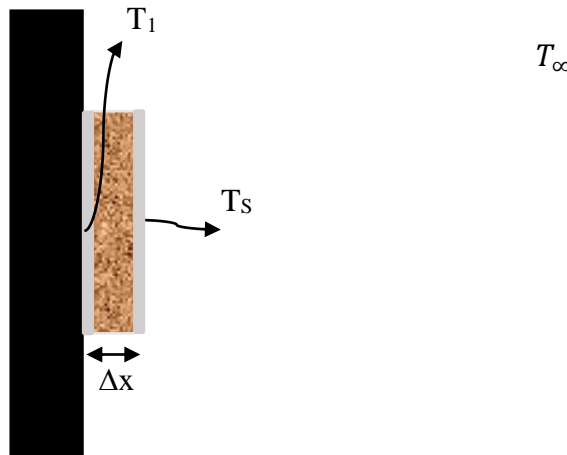


Figure 59 - Layout of the experimental setup with the heating plate and the sample

Therefore, equation 4.4 can be rewritten as:

$$-k * \frac{(T_s - 80)}{20} = h * (30 - T_s) \quad (4.5)$$

The surface temperature of each model, T_s , is measured in the experimental tests, resulting in different convective heat transfer coefficients, h . Consequently, a mean convective heat transfer coefficient is calculated. This will be done in chapter 5 after presenting the experimental surface temperature results for each model. The remaining variable is the combined thermal conductivity of the model. Taking into account that the thermal conductivity of aluminum is 215 W/m.K and that the thermal conductivity of the NL20 Cork agglomerate is 0.044 W/m.K, which equals $215E^{-03}$ W/mm.K and $0.044E^{-03}$ W/mm.K respectively, Fourier's law for conductive heat transfer between the outer faces of both face sheets is once again considered:

$$q = -k_{total} * A * \frac{\Delta T}{\Delta x} = \frac{T_1 - T_3}{\left(\frac{L_1}{k_1 * A} + \frac{L_2}{k_2 * A} + \frac{L_3}{k_3 * A}\right)} \quad (4.6)$$

Where L_1 , L_2 and L_3 correspond to the thicknesses, in mm, of the backside face sheet, the core and the frontside face sheet, respectively. Analogously, k_1 , k_2 and k_3 represent the thermal conductivities of the three parts. The temperature difference between the outer faces of the face sheets is expressed by ΔT and T_1-T_3 . Given that the surface area, A , is the same for all parts and that the temperature difference between the outer faces of the face sheets appears on both sides of equation 4.6, the following simplification is valid:

$$-k_{total} * \frac{1}{\Delta x} = \frac{1}{\left(\frac{L_1}{k_{al}} + \frac{L_2}{k_{NL20}} + \frac{L_3}{k_{al}}\right)} \quad (4.7)$$

All the variables of equation 4.7 are known, except for the total thermal conductivity, k_{total} :

$$-k_{total} * \frac{1}{20} = \frac{1}{\left(\frac{1}{215E^{-03}} + \frac{18}{0.044E^{-03}} + \frac{1}{215E^{-03}}\right)} \quad (4.8)$$

$$k_{total} = 4.889 * 10^{-5} \frac{W}{mm.K} \quad (4.9)$$

Looking at the value above, one can easily conclude that the real thermal conductivity of the assembly is quite close to that of the NL20 cork agglomerate, which meets the expectations given that the assembly is made of 90% of that material.

As mentioned before, heat loss through radiation will be neglected. This can be further explained analyzing the Stefan-Boltzmann Law. For objects other than ideal blackbodies the Stefan-Boltzmann Law is expressed through the following equation:

$$q = \varepsilon * \sigma * A * T^4 \quad (4.10)$$

Where q is the heat transfer per unit time, in Watt, ε is the emissivity of the object, which is dimensionless, σ is the Stefan-Boltzmann constant, in W/m^2K^4 , A is the area of the emitting body, in m^2 , and T^4 represents the fourth power of the absolute temperature, in Kelvin. However, if a hot object is radiating energy to its cooler surroundings, the net radiation heat loss rate can be expressed as:

$$q = \varepsilon * \sigma * A * (T_h^4 - T_c^4) \quad (4.11)$$

Where T_h represents the absolute temperature of the hot object and T_c represents the absolute temperature of the cold surroundings. Once again, since it is a temperature difference, the two temperature variables can be expressed in degree Celsius, °C. Given that the two temperatures, T_h and T_c , are so similar, and despite being raised to the fourth power, the final net radiation heat loss rate value will be very small, thus being negligible.

The numerical analysis of the models relies on the following heat transfer type elements of linear geometric order:

- DC3D8: An 8-node linear heat transfer brick;
- DC3D6: A 6-node linear heat transfer triangular prism;
- DC3D4: A 4-node linear heat transfer tetrahedron.

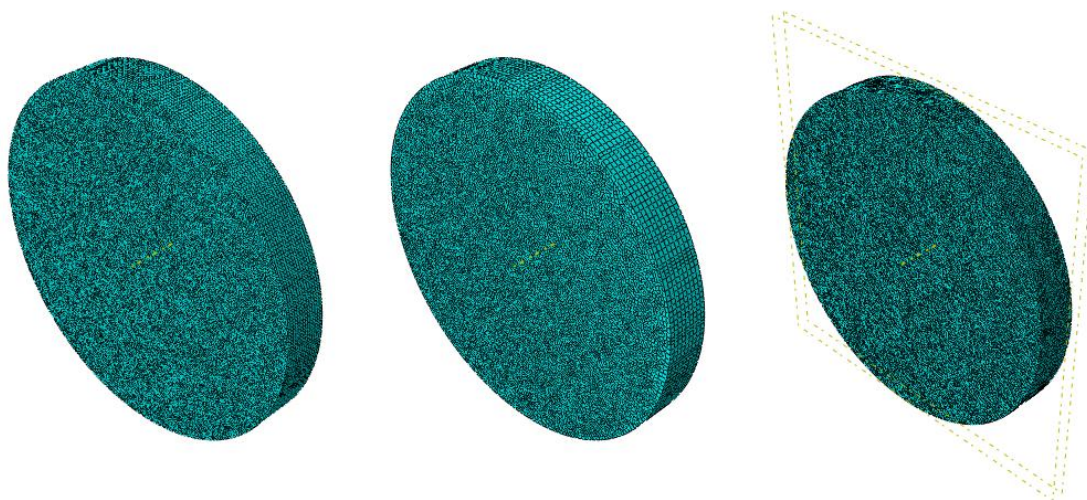


Figure 60 - Hexahedral (l.), wedge (m.) and tetrahedral (r.) element meshes

In some models, such as the 5.14 mm hole pattern model, the hexahedral element is the only one present, which corresponds to the first type, while in other cases, such as the 7 mm hole pattern model, there is a small percentage of wedge elements, the second type mentioned above, due to the existence of regions otherwise unable to mesh. However, the third type, the tetrahedral elements, integrates the free mesh present on both non-through models due to the fact that this is the only possible mesh type applicable. These three mesh types are illustrated in figure 60. It is worth noting that all meshes have been refined around the areas in the vicinity of the holes, taking into account that these are the most critical zones. The non-through models had to be divided into three equally thick partitions, using two datum planes that serve as limits illustrated in in figure 60. This way it is possible to keep the middle partition without any holes or air pockets.

4.2 Mesh Convergence Study

In order to assign the right mesh with the number of elements that meets the desired level of precision, a mesh convergence study was carried out on the 7 mm circular hole model in which the variation of the temperature output as function of the number of elements was analyzed. This model is seen as being representative of all other circular through hole models, the bracket model and the uniform model given its intermediary hole diameter and mesh type, which is the same for all the aforementioned models. Since the assembly is made of essentially two parts, although one part which corresponds to the face sheet was instanced twice into the assembly generating the frontside face sheet and the backside face sheet, there are two different analysis within this convergence study. The first study consists in progressively increasing the number of elements of the core while simultaneously keeping the face sheet elements constant, so that the influence of the core mesh on the temperature output can be evaluated.

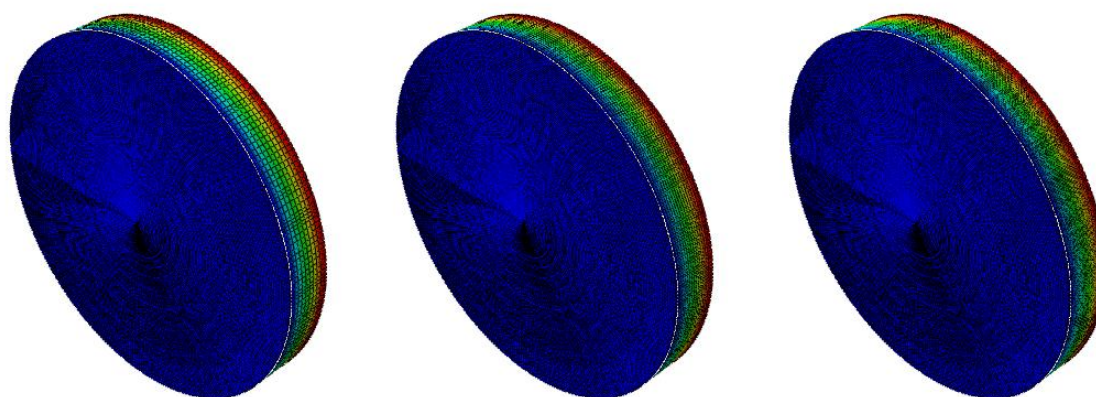


Figure 61 - Core mesh convergence study with 171533 (l.), 270712 and 444728 elements (r.)

In the second study, the face sheet elements will be increased, although on a smaller scale, and the core elements will be kept constant. In both cases, the elements of the core and the elements of both face sheets are summed up, thus giving the total number of elements. At each iteration, the convergence error is calculated between the actual and the previous temperature outputs. Therefore, the convergence error is given by the following equation:

$$\varepsilon_i = \frac{T_i - T_{i-1}}{T_{i-1}} \quad (4.12)$$

Where ε_i stands for the convergence error for iteration i and T_i and T_{i-1} represent the actual and the previous temperature outputs.

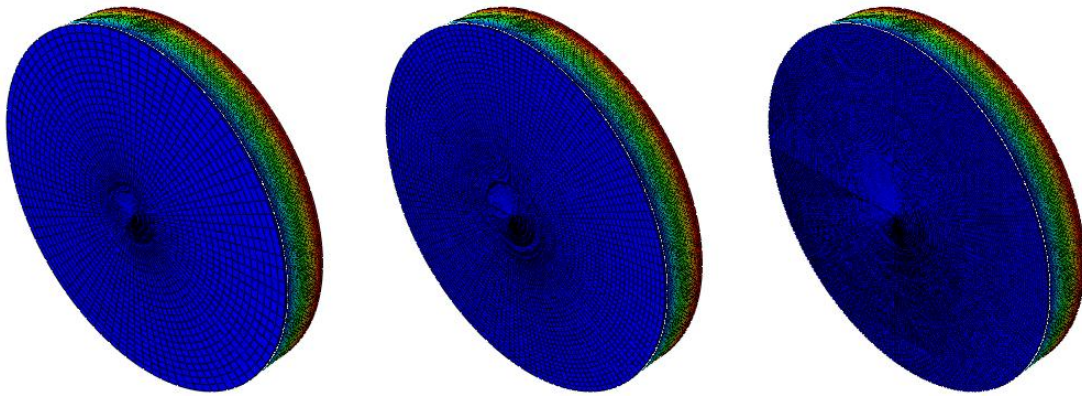


Figure 62 - Face sheet mesh convergence study with 335202 (l.), 341058 and 365746 (r.) elements

Table 7 - Temperature outputs and mesh convergence study for the 7 mm model

Number of elements			Temperature on facesheet [°C]	
Core	Facesheet (x2)	Total		Error [%]
112437	29548	171533	38,876	-
152052	29548	211148	38,873	0,008
164450	29548	223546	38,827	0,118
193470	29548	252566	38,785	0,108
211616	29548	270712	38,751	0,088
238644	29548	297740	38,647	0,268
275960	29548	335056	38,573	0,191
330418	29548	389514	38,561	0,031
385632	29548	444728	38,553	0,021
Facesheet (x2)	Core	Total		Error [%]
2392	330418	335202	37,312	-
5320	330418	341058	38,000	1,844
9588	330418	349594	38,286	0,753
12528	330418	355474	38,336	0,131
14868	330418	360154	38,380	0,115
17664	330418	365746	38,420	0,104
21000	330418	372418	38,475	0,143
26208	330418	382834	38,530	0,143
29548	330418	389514	38,561	0,080
33088	330418	396594	38,583	0,057

In the core mesh study, the first analysis was performed with a relatively unrefined mesh of 112437 elements, increasing the number of elements progressively to 385632 while keeping the number of elements of the face sheets constant, taking into account that this number is multiplied by a factor of 2 in the total number of elements, since there are two face sheets in the assembly. For the core, a mesh of 330418 elements is found to be sufficiently refined, given that it produces a convergence error, in relation to the previous mesh, of less than 0.1%, thus being practicably negligible. In the face sheet mesh study, although the progressive increase of elements is smaller, the change in refinement can be more easily seen (figure 62) as opposed to the core mesh study (figure 61). The result of this study is a mesh of 29548 elements which,

although assumed, had already been used in the core mesh study, with a convergence error that is once again less than 0.1%. While refining the core mesh leads to a lower temperature output, a refinement in the face sheet mesh increases the temperature. It is worth noting that, in order to obtain some primary results for this convergence study and to evaluate the influence of the core mesh and that of the face sheets, a film coefficient had to be assumed. Therefore, the film coefficient value was initially assumed as being 10 W/m².K (Engineering Toolbox, 2014c). This mesh convergence study shows that the influence of the face sheet elements on the temperature is significantly bigger than that of the core elements, given that the reason between the total variations of elements of the two studies is as big as 8.9. In other words, the number of elements of the core study was increased almost nine times the way the face sheet elements were in the face sheet study, but the total variation in temperature in the core study was as low as -0.323°C in comparison to that of the face sheet study, which showed a temperature variation of 1.271°C and is therefore more than three times bigger in module. This effect can be better understood in figure 63.

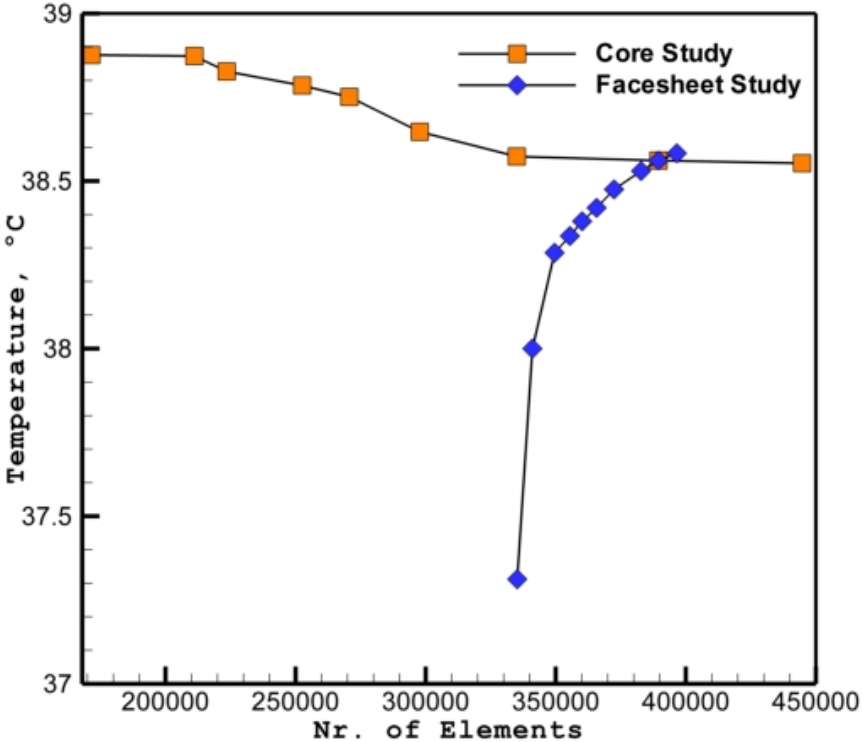


Figure 63 - Core and face sheet mesh convergence study

Figure 63 illustrates that while both the core mesh and the face sheet mesh take some time to converge, the temperature variation in the face sheet mesh study is significantly higher. It should be noted that all points represent the total number of elements of the model. Therefore, the core meshes for the circular through hole models, the bracket model and the uniform model will have approximately 330418 elements while the face sheet meshes will be made of about 29548 elements. The total mesh will be comprised of 389514 elements, which corresponds to the intersection point between the core mesh study and the face sheet mesh study in figure

63. Since there is no method to define the exact desired number of elements in a mesh, the next best approximation will be used.

Another mesh convergence study was carried out for the non-trough hole model without offset, due to the fact that the nature of the meshes, with tetrahedral elements, of this model and the one with offset is different from all the other models, which are comprised of hexahedral or wedge elements, or a combination of both. This will result in a higher number of elements. Since that the face sheet mesh remains the same, there is no need to repeat the face sheet mesh convergence study. Therefore, only the core mesh convergence study is carried out.

Table 8 - Core mesh convergence study of the non-through hole model without offset

Number of elements			Temperature on facesheet [°C]	
Core	Facesheet (x2)	Total		Error [%]
396757	29624	456005	38,783	-
423932	29624	483180	38,783	0,000
543065	29624	602313	38,770	0,034
620166	29624	679414	38,764	0,015
733878	29624	793126	38,752	0,031
854703	29624	913951	38,744	0,021
942392	29624	1001640	38,753	0,023
1314495	29624	1373743	38,738	0,039

Table 8 shows that the core mesh of the non-through hole model without offset converges rather quickly, judging by the total temperature variation, which is of 0.045°C in module, resulting in very small and thus practicably negligible convergence error values. Therefore, taking into account the demanding computational requirements and the required time to run the analysis, a core mesh with 733878 elements is found to be satisfactory, which combined with the face sheets meshes, results in a total mesh comprised by 793126 tetrahedral elements, which in turn corresponds to slightly more than double of the elements present in the total mesh of the 7 mm circular hole model in table 7. Similarly to the previous core mesh convergence study, there is a decrease of the temperature output as the number of elements goes up.

Chapter 5 - Results and discussion

5.1 Experimental Results

Shortly after the heating plate reached the desired temperature of 80°C, the temperature on the center of the top face sheet of each test sample was measured through the contact thermocouple, as illustrated in figure 65. The measurement of each test sample took a few moments due to the stabilization time of the thermocouple. The ambient temperature, which in this case corresponds to the sink temperature, was measured and established as being 30°C.



Figure 64 - Temperature measurement of the heating plate

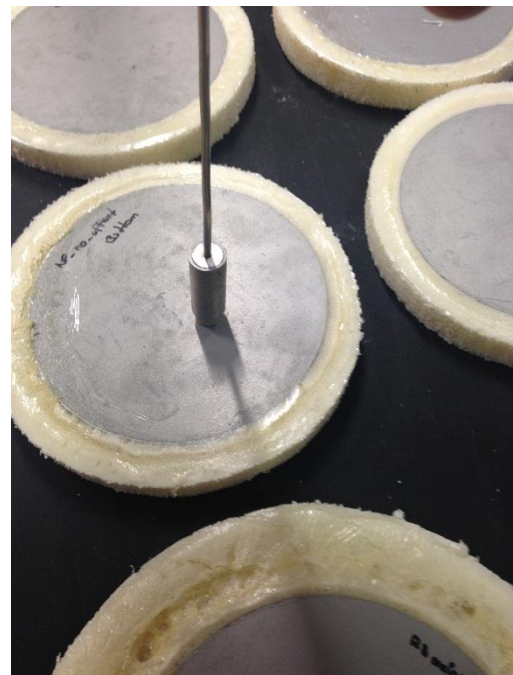


Figure 65 - Temperature measurement of the test samples

The temperature measurement of all test samples took about 10 minutes. There were no signs of any melting by the polyurethane foam, which served as a good enough thermal insulator given that its temperature was only slightly higher than the ambient temperature after the tests were completed. The temperatures of the test samples are illustrated in the bar chart in figure 66. There is a correspondence between the purpose study of the test sample and the bar color. While the blue bars represent the hole shape, or lack thereof, assessment, the red bars represent the study of the hole diameter influence. Within the hole diameter study is also the mass influence study, which is represented by the orange bars. Finally, the turquoise bars stand for the study of the effect of non-through holes and the existence of a slight offset between the hole patterns on each side. The core configuration that immediately stands out as the worst insulator is the 10 mm circular hole pattern configuration. On the other hand, the non-through

hole with offset configuration seems to be the most insulating, with the uniform configuration's performance differing only 0.1 °C from it. Relatively to the red and orange bars, increasing the hole diameter apparently leads to a temperature increase, meaning that it reduces the insulating ability of the cores. Besides that, the orange bars show that having a bigger fraction of cork leads to a lower temperature, thus increasing the insulating ability.

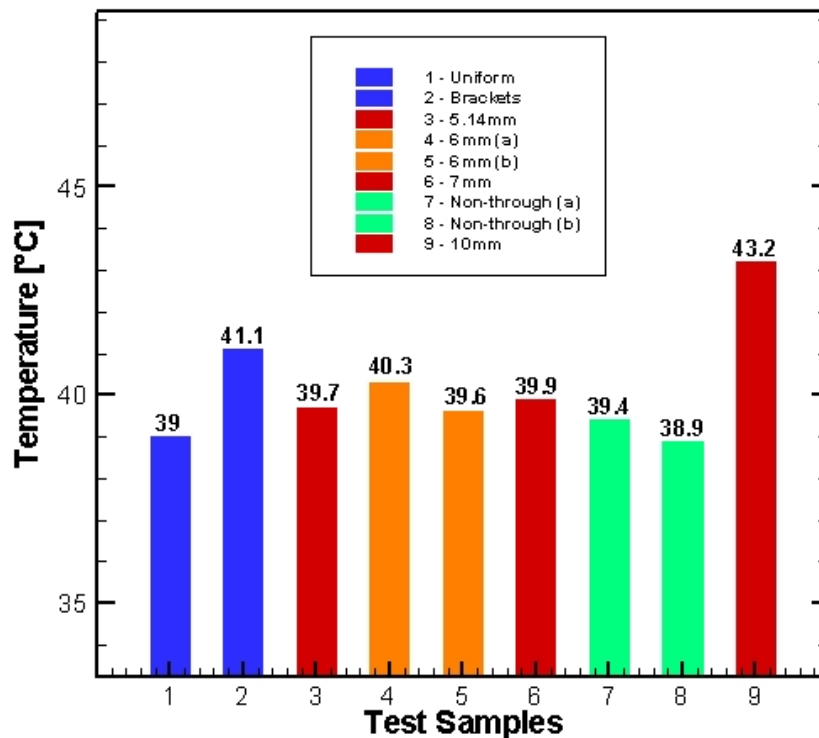


Figure 66 - Bar chart of the experimental results

Looking at the turquoise bars, it seems that the existence of the offset between the non-through holes, even if small, has a beneficial effect on the overall insulating ability of the core. Finally, the blue bars show that the bracket shaped holes are not as insulating as the circular ones and the uniform sample registered a lower temperature than all the through-hole models. This means that the existence of holes and air pockets, which was expected to be beneficial due to the air's lower thermal conductivity, is actually a detrimental factor to the insulating ability of the core.

The thermal image recorded by the infrared camera, illustrated in figure 67, shows the temperature distribution on the top face sheets of the samples. The image shows the heating plate upside down, relatively to figure 43 in chapter 3. The samples have the same number as in the bar chart above so that they could be identified in the image. Once again, the test sample that immediately stands out is the 10 mm circular hole sample, marked with number 9, which shows a temperature distribution unlike any other test sample. While its colors indicate a temperature of about 37 °C, the more exact temperature is given by the contact thermocouple, shown in the bar chart of figure 66.

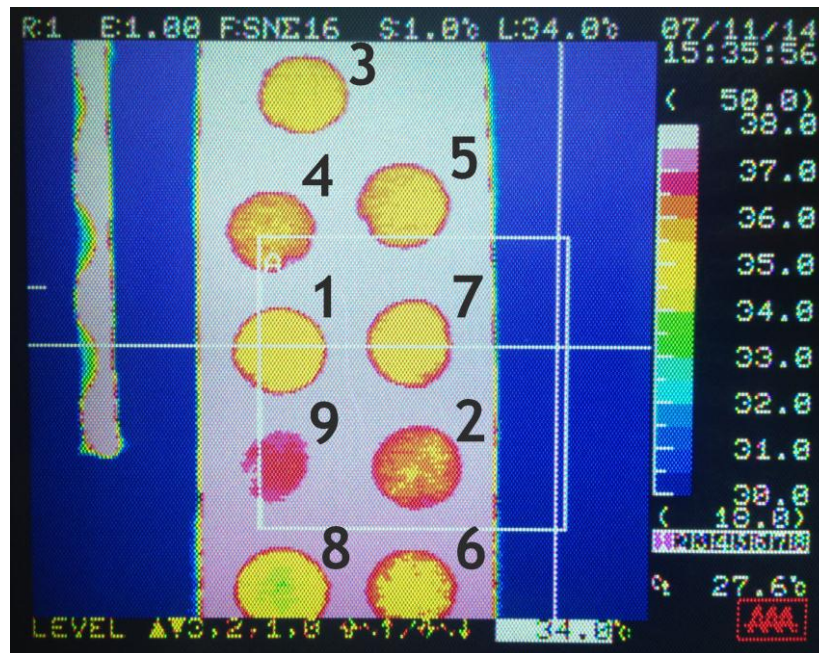


Figure 67 - Thermographic image taken from the infrared camera above

However, it is clear that every test sample has its higher temperatures at the edge and although the polyurethane foam is known to be a good insulator, some heat losses were already expected. Sample 2 seems to have the second worst thermal insulating ability, judging by its temperature distribution, followed by sample 4, which correspond to the bracket pattern sample and the lighter version of the 6 mm circular hole model, respectively. On the other hand, sample number 8, which is the non-through hole sample with offset, looks like the best insulator, being the only one presenting a slightly green area in the center of the top face sheet. The uniform sample marked with number 1, although having registered a similar temperature, does not present any green areas in its temperature distribution. The remaining models present temperatures within the same range, which can be confirmed by the bar chart that shows a difference of no more than 0.5°C between them.

The thermal image in figure 68 has a different color range that goes up to 40°C, in other words, a difference in 2°C in color range causes a significant change in the color of the test samples. This was done in order to turn the 10 mm circular hole sample, sample 9, more visible. This in turn led to a color change mostly from yellow to green on the other samples. However, samples 1 and 8, which correspond to the uniform and the non through hole with offset samples, present a blue area in the center, proving once again to have the most insulating ability. The heterogeneities in the temperature distribution in sample 9 are mainly due to the polyurethane foam excess on the top face sheet that could not be removed without damaging the aluminum. Samples 2 and 4, corresponding to the bracket pattern sample and the lighter version of the 6 mm circular hole sample, have the highest temperatures, except for the 10 mm circular hole sample.

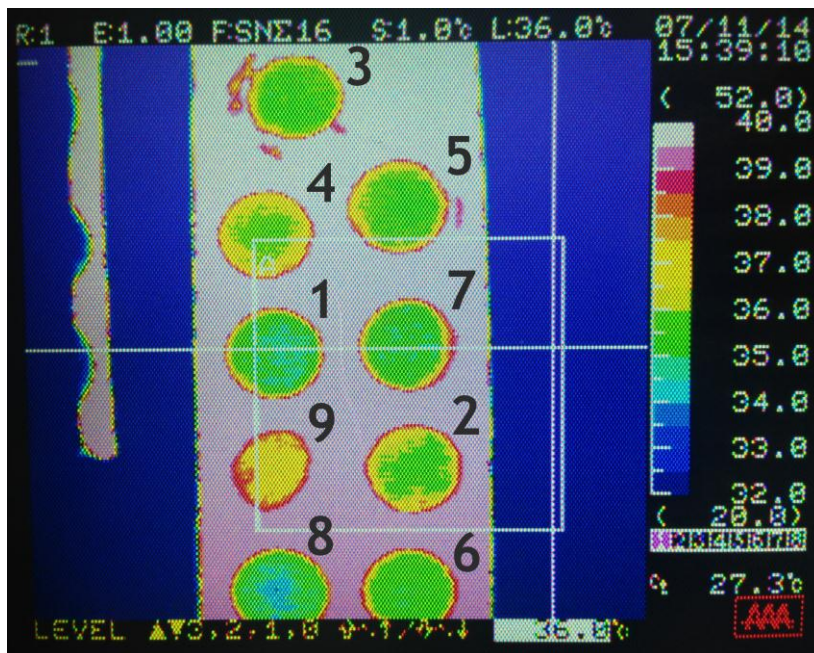


Figure 68 - Thermographic image with temperature range up to 40°C

The temperature range was once again changed, being 34°C and 42°C the lowest and the highest temperature values, respectively. Although there are still some yellow and green zones, the sample colors have for the most part changed from green to blue. In this case, the superiority of the non-through hole offset sample, marked with number 8, in relation to all others can be clearly identified by the dark blue zone that covers almost all of the top. Samples 1, 6 and 7, which are the uniform, the 7 mm circular hole and the non-through hole without offset samples, also present slightly darker blue areas even though not with the same magnitude.

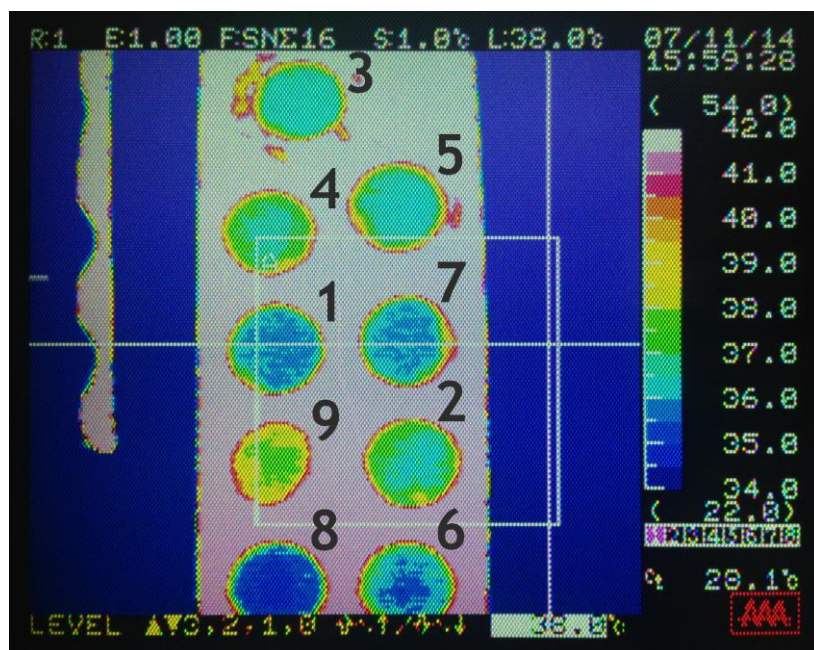


Figure 69 - Thermographic image with temperature range up to 42°C

Once again one can clearly see the difference in temperature distribution that the 10 mm circular hole sample, marked with number nine, has relatively to all the other samples, not presenting any blue areas whatsoever. Based on these results and observations taken from the experimental thermal tests, the hole diameter study, the cork mass study and the non-through hole study, the following conclusions can be drawn:

- The effect that the air's convection has on the insulating ability of the core is bigger than initially expected, judging by the results from the 10 mm circular hole sample. Besides that, the effect of the convection of air was believed to be beneficial to the insulating ability, given that heat transfer through conduction is significantly higher than through convection, but the results show that the bigger the hole diameter, which means bigger volumes of air, the higher the temperature on the top face sheet. Consequently, the insulating ability decreases.
- The cork mass study shows that the bigger the fraction of cork, the more thermally insulating the core becomes. The "heavier" version of the 6 mm circular hole sample has a lower temperature on the top face sheet than the "lighter" version. On the other hand, the uniform sample, which is the heaviest model and has no holes in its configuration, presents a lower temperature than both of those samples.
- The effect that the glue mixture used to join the face sheets and the core has on the insulating ability is unknown, but can be investigated by comparing the experimental results with the numerical ones.
- The non-through hole configuration, whether it has an offset between the hole patterns on each side or not, shows itself to be the best alternative to the uniform configuration, due to the fact that it has lower mass and retains its insulating properties. In the case of the non through hole sample with offset, the temperature on the center of the top face sheet is actually lower than in the uniform sample and although the difference is of only 0.1°C , the thermal image in figure 69 shows a significant discrepancy in the temperature distribution of these models.
- In none of the thermal images previously shown, the hole patterns were recognizable through the aluminum face sheet by looking at the temperature distribution.

5.2 Numerical Results

As mentioned earlier in chapter 4, the numerical analysis could only be carried out correctly after experimentally determining the convective heat transfer coefficient and in order to achieve that the experimental temperature results had to be known. Thus, it is now possible to determine the convective heat transfer coefficient for each model via equation 4.5. Table 9 shows the calculated convective heat transfer coefficient, or film coefficient, for each model.

Table 9 - Calculated convective heat transfer coefficient for each test sample

Model description	Surface Temperature [°C]	Film coefficient [W/mm ² .K]
Uniform	39	11,1355E ⁻⁶
Bracket pattern	41,1	8,56637E ⁻⁶
5.14 mm	39,7	10,1556E ⁻⁶
6 mm (a)	40,3	9,42158E ⁻⁶
6 mm (b)	39,6	10,2868E ⁻⁶
7 mm	39,9	9,90101E ⁻⁶
Non-through (a)	39,4	10,5577E ⁻⁶
Non-through (b)	38,9	11,2881E ⁻⁶
10 mm	43,2	6,81466E ⁻⁶

The higher the surface temperature, the lower the film coefficient will be. The mean film coefficient resulting from the values from table 9 is 9.79193E⁻⁶ W/mm².K, which equals 9.79193 W/m².K. This will be the selected film coefficient value included in the numerical analysis. This also means that the initially assumed convective heat transfer coefficient (10 W/m².K) for the mesh convergence studies in chapter 4 was very close to the real value. Now that the real convective heat transfer coefficient is known, the numerical analysis can be carried out for each model. A job file, which contains the log and all the information of the numerical analysis, was created for each model.

Table 10 shows the numerical results for each model and compares them to the corresponding experimental results. The precision of the numerical analysis in relation to the experimental results differs between models. Curiously, in the case of the two models that showed the best results in the thermal tests, the numerical and experimental results are almost identical. Therefore, the numerical results confirm the superiority of the uniform and the non-through hole with offset models in thermal insulating ability relatively to all other models. However, according the numerical results, there is one model that surpasses both the uniform and the non-through hole with offset models, which is the 10 mm circular hole model. In the experimental results, this was the model with the worst results, thus proving that the air convection and the effect that it has on the insulating ability are not considered in the numerical results.

Table 10 - Numerical Results versus Experimental Results

Model description	Numerical Temperature [°C]	Real Temperature [°C]
Uniform	38,988	39
Bracket pattern	38,873	41,1
5.14 mm	38,771	39,7
6 mm (a)	39,214	40,3
6 mm (b)	39,442	39,6
7 mm	39,030	39,9
Non-through (a)	38,936	39,4
Non-through (b)	38,900	38,9
10 mm	38,672	43,2

It seems that the models with bigger fractions of cork and minimum air convection effect, like the uniform model, the 6 mm circular hole model with more mass, which is the (b) version, and both non through hole models are the ones with the lowest discrepancies between the numerical and the experimental results, while the bracket model, the (a) version of the 6 mm circular hole model and the 7 mm and 10 mm circular hole models, which have bigger fractions or volumes of air, present bigger differences. However, the model with the smallest hole diameter, which is the 5.14 mm circular hole model, also presents a discrepancy of approximately 1°C. For more details on the numerical results, see Annex B. The bar chart in figure 70 accurately displays the discrepancy between the numerical and experimental results in some models, and the precision in others.

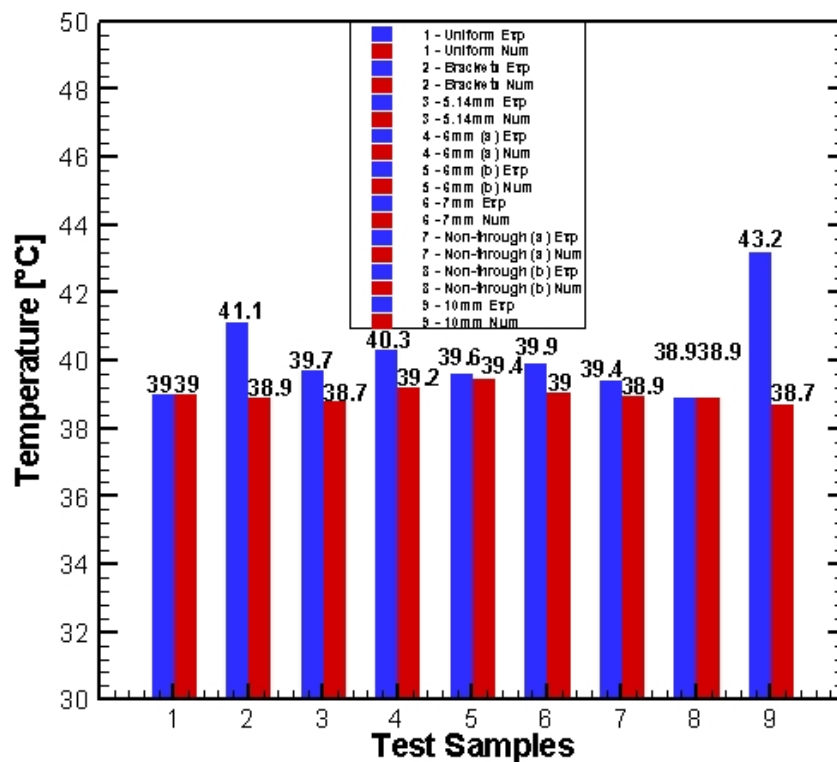


Figure 70 - Bar chart of the numerical and experimental results

The bar chart above shows that in every sample, the experimental temperature is either bigger or equal to the numerical temperature. This once again shows that there are factors in the real situation that are not taken into account in the numerical scenario, such as the effect of the glue mixture and the air convection. However, in the numerical results, and taking into account that the all the models are perfectly thermally insulated on the sides, the temperature distribution on the face sheet is uniform, as illustrated in figure 71.

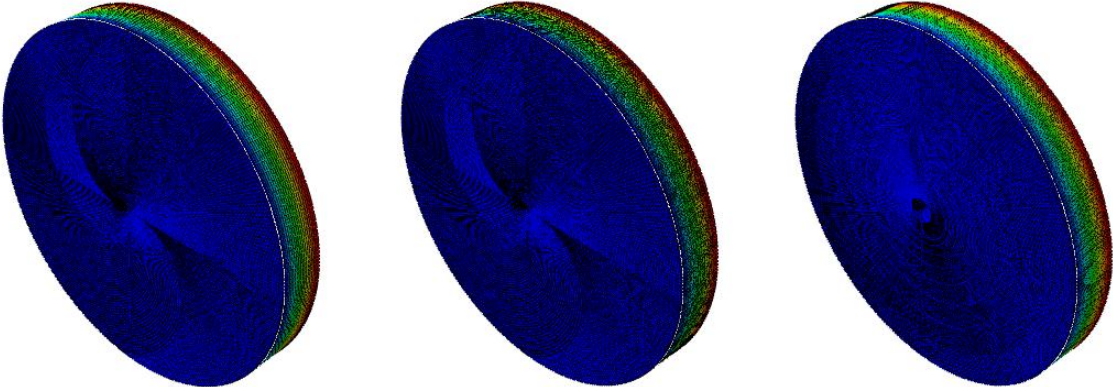


Figure 71 - Temperature distributions for the uniform, non-through hole with offset, and 10 mm circular hole models (l. to r.)

A zone of interest was selected for the 10 mm circular hole model in which the thickness of the sample was reduced to a minimum value in order to study the temperature values of the face sheet with more precision. Figure 72 shows that the temperature distribution on the outer side of the face sheet remains uniform. On the other hand, the inner side shows five sections, each one with a different thickness associated to it.

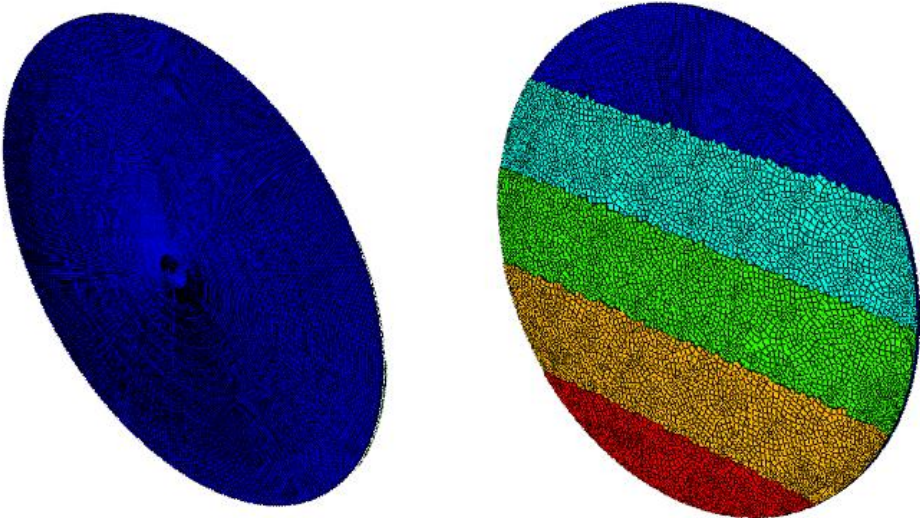


Figure 72 - Outer and inner sides of the front side face sheet

The upper section, in dark blue, shows the inner side of the face sheet, while the remaining section below become progressively thicker with the cork core. Each section has a different color, and thus a different temperature. The holes are included in the sections although they are not visible due to the fact that they are represented by cylindrical solids with the properties of air. The progressiveness of the temperature through the thickness of the core can be better understood by looking at figure 73. While the left side shows the front side face sheet, the right side already shows the inner side of the face sheet in the back. At first glance, the temperature seems to vary uniformly with the thickness of the core. The air sections, representing the holes, apparently do not interfere with the evolution of the temperature since that there are not any visible variations in the temperature layers represented by the different color columns.

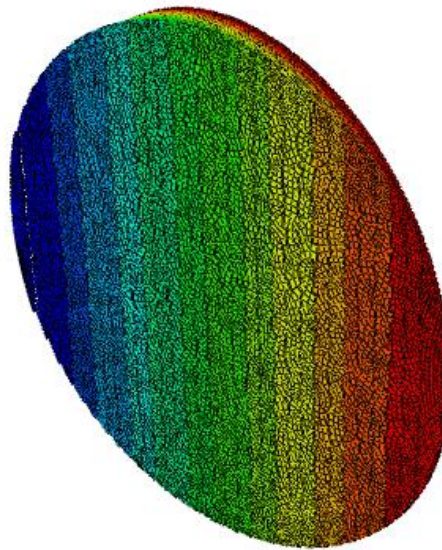


Figure 73 - Temperature layer evolution through the thickness of the core

Although theoretically the temperature is the same in any point of the face sheet and the color evolves uniformly through the thickness, the temperature profile through the thickness may not be the same for every model. Therefore, a set of points along the thickness, known as path, was selected for each model in order to study their temperature profiles. Figure 74 shows the temperature variation along the thickness of the core of each model, starting from the heated side. Notice that only the core thickness is considered, thus the maximum value being 18 mm in the bar chart below. It is worth noting that in all the models, except for the uniform model, the path of chosen points deliberately crosses the hole sections in order to investigate the effect that the holes and the consequent change of properties have on the temperature profiles. It is possible to conclude through figure 74 that in all models, except for both non-through hole models, the temperature does in fact vary uniformly along the thickness of the core given that these models present straight lines although with slightly different slopes. In the case of the non through hole models, the temperature profile presents a curve.

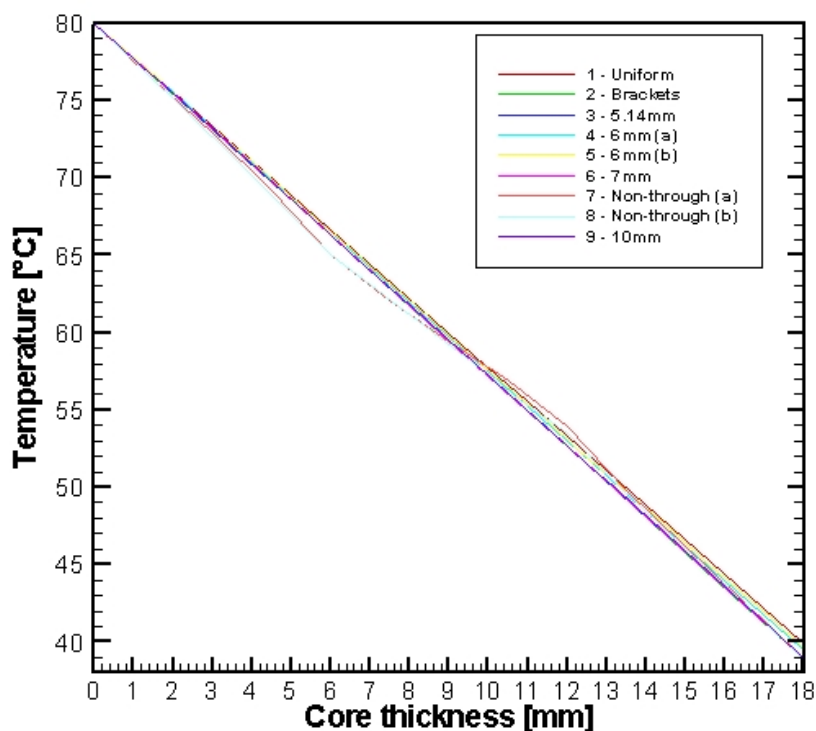


Figure 74 - Temperature profiles through the thickness of each model

This does not necessarily mean that there are some irregularities in the middle section of the core, because the mesh type for these two models is different than the others. Therefore, the mesh itself can be at the origin of these irregularities. Taking into account all the aforementioned theoretical results and studies, the numerical analysis led to the following conclusions:

- The two models with the lowest temperatures on the top face sheet, and thus with the best results in terms of thermal insulating ability, in the experimental tests are the uniform and the non through hole with offset models. The superiority in insulating ability of these models relatively to all others was confirmed by the numerical analysis, presenting practically no discrepancy whatsoever between numerical and experimental results.
- The 10 mm circular hole model is the best insulating model in the numerical analysis while simultaneously being the worst in the experimental tests. Therefore, given that the air convection is not taken into account in the numerical analysis, the discrepancy between the numerical results and the experimental ones confirm the magnitude of the effect that this phenomenon has on the overall insulating ability. This discrepancy is almost nonexistent in the models with bigger cork fractions where the air convection is strongly limited. The introduction of large air volumes in the cork core, even though having a lower thermal conductivity, decreases the insulating ability.

- The glue mixture on the other hand has little or no effect on the models given that it is present in all of them and some, like the uniform and the non through hole model with offset, do not present differences between the numerical results and the experimental results.
- With the models being thermally insulated on the sides, the temperature will remain the same on any point of the face sheet, which in turn leads to a uniform temperature distribution. This is practically impossible to achieve in the experimental tests, which led to irregularities in the temperature distribution of the models.
- The temperature varies evenly, or uniformly, along the thickness of the cores of every model except the non through hole models, which present a slight curve instead of straight lines. This in turn could be caused by the difference in the mesh type. However, the hole sections or air volumes do not interfere in the temperature profile.

Chapter 6 - Conclusions and future research

6.1 Final conclusions

The present work allowed to assess the feasibility of employing a specific type of cork agglomerate, which is a natural and environmentally friendly material, as the core material for sandwich structures in the form of a panel with aluminum face sheets. A set of conceptual design possibilities for the cork agglomerate core was studied and put through experimental thermal tests. In addition to those tests, computational studies were conducted based on numerical analysis on the finite element code ABAQUS® v6.10-1. The comparison between the experimental results and the numerical ones led to the following conclusions:

- Seeing that one of the key objectives of the project in which the present work is inserted is, in addition to the implementation of more environmentally friendly materials, the weight reduction of the structural parts and although air is a better thermal insulator than cork, the existence of through-holes in the cork configuration is actually a detrimental factor to the overall insulating ability of the sandwich panel. This is mainly due to the convective movement of air inside the holes which was not taken into account in the numerical analysis, which in turn led to discrepancies between the experimental results and the numerical ones, especially in the case of the circular through-hole models with bigger hole diameters and consequently bigger volumes of air, such as the 10 mm model. For this reason, models such as the “lighter” version of the 6 mm circular hole model, which were initially expected to be good solutions and presented satisfactory results in the numerical analysis, ended up to have the worst insulating abilities in the experimental tests, in addition to the 10 mm circular hole model. Although the bracket model is the only model that was tested with a different hole shape, the results show that the circular model is the best option when it comes to the shape or form of the hole.
- The mass study shows that the bigger the fraction of cork in the core, the smaller the effect of air convection and consequently the better the insulating ability of the sandwich panel. This of course means more weight. Knowing that one of the key objectives of the present work is lowering the weight of the core by the application of hole patterns without compromising its insulating properties, increasing the fraction of cork in the core would lead to the exact opposite. Therefore, the non-through hole core configuration shows itself to be the best compromise between weight reduction and thermal insulating. While having holes in its configuration, it avoids the air’s convection inside the hole by essentially dividing the air pocket in two. The results

show that while the non-through hole model with offset is 11% lighter, it is as good an insulator as the uniform model. The effect of introducing a slight offset between the holes between each side, even if small, has a beneficial effect on the insulating ability of the core.

- Although not being developed within the scope of the DesAir Project for their thermal insulating properties but rather for their mechanical, acoustic and vibratic aspects, the test results show that these core configurations are proven to be a very good alternative to the conventional insulating solutions. The presence of air in the core's cellular membranes, the cell size and the slow burn rate account for its competitiveness in insulating ability. The demand of the global stake holders to reduce by 75% the environmental impact, such as the CO₂ emissions, associated to the current manufacturing, operational and maintenance technologies supports the use of natural materials such as cork due to its 100% ecological nature.

6.2 Prospects for future developments

The many advantages of sandwich constructions, the development of new materials, and the need for high performance, low-weight structures insure that sandwich construction will continue to be in demand. Sandwich construction is expected to continue to be the primary structure for satellites. In aircraft, it will be increasingly used particularly for large aircraft. Besides that, alternative sources of energy such as wind energy mill systems are being developed which rely heavily on composite sandwich constructions. On the other hand, cork and other natural materials will continue to be explored. Although the cork industry and the public in general have viewed cork mainly in terms of stoppers, new cork composites can be foreseen for structural purposes, as well as new applications. This is mainly due to the specific cork material characteristics. As for cork agglomerates, these are expected to be further developed by using densification techniques which confer to cork different mechanical, thermal, acoustic or vibratic properties while simultaneously maintaining its ecological characteristics. Pereira reports that there's the possibility of cork, which is a good electrical insulator, being used as a porous dielectric by filling its cells with gas, which in turn would provide the ability of retaining an electrical charge, thus behaving like a piezoelectric that could be used to develop smart sensors (Pereira, 2007). Relatively to the present work, the tests and analysis carried out as well as the previously shown results should be seen as a preliminary step which serves as motivation for future developments concerning this area of study. Therefore, the following suggestions should be taken into account:

- Since that there was only one model that was tested with a different hole shape, which was the bracket model, a bigger variety of hole configurations should be developed,

tested in compared to the uniform model, the circular hole models and between each other in order to further investigate the influence that the hole shape has on the insulating ability of the models.

- Given that the results show the non through hole model to be the best compromise or combination between mass reduction and thermal insulation ability, this core configuration should be further explored. The influence of the depth of the holes, on each side, on the insulating ability should be assessed as well as the effect of the hole diameter. Increasing the number of holes while decreasing the hole diameter would maintain the weight and further mitigate the effect of the air convection. Although the effect of the offset between the holes on each side was tested and proven to be beneficial, only one offset value in the horizontal direction was tested. Therefore, different offset values not only in the horizontal direction but also in the vertical direction should be introduced and explored.
- It is worth noting that all of the models were made of the same NL20 cork agglomerate. Therefore, models with the same core configuration but consisting of different cork agglomerates should be tested and compared to each other. Cork agglomerates with higher internal porosity could improve the insulating ability, in addition to having a lower weight.
- Although in chapter 4 the effect of the radiation on the temperature results was proven to be practicably negligible, this phenomenon should be taken into account in future analysis in order to achieve more exact results. In addition to the radiation aspect, future numerical analysis should also integrate and focus on the effect of the air convection inside the holes in an effort to eliminate or reduce it to a minimum. This study should be carried out by resorting to other codes such as the ANSYS® Fluent computational fluid dynamics, or CFD, software and its results should be compared to those of the present work.

References

Allen, H. G.; (1969) "Analysis and Design of Structural Sandwich Panels". Oxford New York, Pergamon.

Amorim Cork Composites; (2009) "CoreCork by Amorim: Technical Data", Amorim Cork Composites, Amorim.

Beausoleil-Morrison I., Mitalas, G., Chin, H.; (1995) "Estimating Three-Dimensional Below-Grade Heat Losses from Houses Using Two-Dimensional Calculations", *Thermal Envelopes IV, CANMET, Canada*.

Bert, C.W.; (1991) Part I and II, Shock and Vibration Digest, Vol. 23, pp. 3-14, 19-21.

Beckwith, S. W.; (2008) "Sandwich Core Materials & Technologies - Part I", SAMPE Journal, Vol. 44, No. 4, pp. 30-31.

Bitzer, T.; (1997) "Honeycomb Technology", Hexcel Corporation, Chapman & Hall, Springer.

Carlsson, L. A., Kardomateas, G. A.; (2011) "Structural and Failure Mechanics of Sandwich Composites", Solid mechanics and its applications, Vol. 121, Springer, New York.

Carvalho, P.; (2008) "Análise do comportamento mecânico e identificação do tipo de falha em estruturas sandwich com núcleos de cortiça", MSc dissertation, Instituto Superior Técnico, Lisbon.

Castro, O., Silva, J. M.; (2010) "Cork agglomerates as an ideal core material in lightweight structures", Materials and Design, Vol. 31, pp. 425-432.

Chiebao, F.; (2011) "Technical Manual: Cork Construction & Decoration Materials", Technical Data Sheet, APCOR: Santa Maria de Lamas.

Costa, I.; (2009) "Estudo do Comportamento de Estruturas Sandwich com Núcleos de Cortiça para Pás de Turbinas Eólicas", MSc dissertation, Faculdade de Engenharia da Universidade do Porto, Oporto.

Du, Y., Yan, N., Kortschot, M. T.; (2012) “Light-weight honeycomb core sandwich panels containing biofiber-reinforced thermoset polymer composite skins: Fabrication and evaluation”, *Composites: Part B*, Vol. 43, pp. 2875-2882.

Engineering Toolbox; (2014a) “Densities of Miscellaneous Solids”, Aluminum, http://www.engineeringtoolbox.com/density-solids-d_1265.html, last access: June 10, 2014.

Engineering Toolbox; (2014b) “Thermal Conductivities of some common Materials and Gases”, Aluminum, http://www.engineeringtoolbox.com/thermal-conductivity-d_429.html, last access: June 10, 2014.

Engineering Toolbox; (2014c) “Convective Heat Transfer Coefficients”, Free Convection - Air, http://www.engineeringtoolbox.com/convective-heat-transfer-d_430.html, last access: June 15, 2014.

Esteves, D.; (2010) “Desenvolvimento, caracterização e avaliação do comportamento termo-mecânico de um novo material constituído principalmente por cortiça”, MSc dissertation, Instituto Superior Técnico, Lisbon.

FAA; (2012) “Chapter 7: Advanced Composite Materials”, *Aircraft Maintenance Technician Handbook*, Volume 1, Federal Aviation Administration, U.S. Department of Transportation, Oklahoma City

Fairbairn, W.; (1849) *An Account of the Construction of the Britannia and Conway Tubular Bridges*, John Weale, London.

Gil, L.; (1998) “Cortiça - Produção, Tecnologia e Aplicação”, Ed INETI, Lisbon.

Gil, L.; (2000) “História da Cortiça”, Santa Maria de Lamas: APCOR, Portugal.

Gil, L., Silva, P.; (2000) “Cork Composites”, *ECCM9-Composites: From Fundamentals to Exploitation*, Brighton, UK.

Gil, L.; (2007) “Cork as a building material - Technical manual”, First Edition, Santa Maria de Lamas: APCOR.

Gil, L.; (2009) “Cork Composites: A Review”, *Materials* 2, no. 3: 776-789.

Ha, K.H.; (1989) "Finite Element and Sandwich Construction: A Critical Review," Sandwich Constructions I Proceedings of the First International Conference on Sandwich Construction, EMAS Publications, United Kingdom, pp. 69-84.

Herrmann, A.S., Zahlen, P. C., Zuardy, I.; (2005) "Sandwich Structures Technology in Commercial Aviation", Sandwich Structures 7: Advancing with Sandwich Structures and Materials, 13-26. Airbus Deutschland GmbH.

Hexcel Composites; (2000) "HexWeb™ Honeycomb sandwich design technology", Publication No. AGU 075b, Hexcel Composites, Duxford.

Hoff, N.J.; (1950) "Bending and Buckling of Rectangular Sandwich Plates". N.A.C.A. Technical Note 2225.

Libove, C., S.B. Batdorf; (1948) "A General Small Deflection Theory for Sandwich Plates," NACA Report 899, Washington, D.C.

Megson, T. H. G.; (2010) "An Introduction to Aircraft Structural Analysis", Elsevier Ltd., Oxford.

Mestre, A., Gil, L.; (2011) "Cork for Sustainable Product Design", *Ciência & Tecnologia dos Materiais*, Vol. 23, n. 3/4.

Noor, A.K., W. Scott Burton, C.W. Bert; (1996) "Computational Models for Sandwich Panels and Shells," *Applied Mechanics Reviews*, Vol. 49, No. 3, pp. 155-199.

Pereira, A.; (2012) "Cork and Sustainability: Discussing the Sustainable Use of the Material from a Design Perspective", *Journal of Shanghai Jiaotong University (Science)*, Volume 17, Issue 3, pp 360-363.

Pereira, H; (2007) "Cork: Biology, Production and Uses", Universidade Técnica de Lisboa, Elsevier publishing, The Netherlands.

Plantema, F.J.; (1966) "Sandwich Construction: The Bending and Buckling of Sandwich Beams", Plates and Shells, John Wiley and Sons, New York.

Reis, L., Silva, A.; (2009) "Mechanical Behavior of Sandwich Structures using Natural Cork Agglomerates as Core Materials", Instituto Superior Técnico, Lisbon.

Ricardo, J.; (2009) "Structural Modelling Validation of Cork Composites for Aeronautical Applications", MSc dissertation, Instituto Superior Técnico, Lisbon.

Sargianis, J., Kim, H.-I., Andres, E., Suhr, J.; (2012a) "Sound and Vibration Damping Characteristics in Natural Material based Sandwich Composites". *Composite Structures*, doi: <http://dx.doi.org/10.1016/j.compstruct.2012.09.006>

Sargianis, J., Kim, H. & Suhr, J.; (2012b) "Natural Cork Agglomerate Employed as an Environmentally Friendly Solution for Quiet Sandwich Composites". *Sci. Rep.* 2, 403; DOI:10.1038/srep00403

Sika; (2007) "Sika Boom[®]-S, 1-part expansive fixing, filling, and insulating adapter foam", Product Data Sheet, Sika, Turkey.

Silva, J.M., Gamboa, P.V., Nunes C., Paulo L. & Franco, N.; (2011) "Cork: Is It a Good Material for Aerospace Structures?", Structures, Structural Dynamics and Materials Conference, Denver, Colorado.

Silva, S.P., Sabino, M.A., Fernandes, E.M., Correlo, V.M., Boesel, L.F., Reis, R.L.; (2005) "Cork: properties, capabilities and applications", *International Materials Reviews* 2005; Vol. 50, No. 6, pp. 345-65.

Soares, B.; (2007) "Estruturas sandwich com utilização de núcleos de cortiça", MSc dissertation, Instituto Superior Técnico, Lisbon.

Vamja, D. G., Tejani, G. G.; (2012) "Analysis of composite material (sandwich panel) for weight saving", *International Journal of Engineering Research and Technology*, Vol. 1 (02), ISSN 2278 - 0181.

Veras, M.; (2013) "Estudo, Fabrico e Caracterização de Painéis Sanduíche com Núcleos em Materiais Compósitos de Cortiça", Instituto Superior de Engenharia de Lisboa, Lisbon.

Vinson, J.R.; (1999) "The Behavior of Sandwich Structures of Isotropic and Composite Materials", University of Delaware, Newark, Technomic Publishing Co. Inc..

Vinson, J.R.; (2005) "Sandwich Structures: Past, Present, and Future", *Sandwich Structures 7: Advancing with Sandwich Structures and Materials*, 3-12, Springer.

Annex A - Sandwich material properties

Table A. 5 - Properties of typical facing materials for sandwich panel construction (Hexcel Composites, 2000).

FACING MATERIAL	TYPICAL STRENGTH Tension/Compression MPa	MODULUS OF ELASTICITY Tension/Compression GPa	POISSON'S RATIO μ	TYPICAL CURED PLY THICKNESS mm	TYPICAL WEIGHT PER PLY kg/m ²
Epoxy UD CARBON tape (0°) 60% volume fraction	2000 / 1300	130 / 115	0.25	0.125	0.19
Epoxy UD GLASS tape (0°) 55% volume fraction	1100 / 900	43 / 42	0.28	0.125	0.25
Epoxy WOVEN CARBON (G793-5HS) 55% volume fraction	800 / 700	70 / 60	0.05	0.30	0.45
Epoxy WOVEN ARAMID (285K-4HS) 60% volume fraction	500 / 150	30 / 31	0.20	0.20	0.27
Epoxy WOVEN GLASS (7781-8HS) 50% volume fraction	600 / 550	20 / 17	0.13	0.25	0.47
Phenolic WOVEN GLASS (7781-8HS) 55% volume fraction	400 / 360	20 / 17	0.13	0.25	0.47
ALUMINIUM Alloy 2024 T3 5251 H24 6061 T6	Av. Yield 270 150 240	Av. 70	0.33	0.50	1.35
STEEL carbon 1006 1017	Av. Yield 285 340	Av. 205	0.30	0.5	4.15
Exterior PLYWOOD Fir	30 / 35	Av. 9	0.1	12.7	6.3
Tempered HARDWOOD Teak	110 / 40	Av. 12	0.1	12.7	8.5

Table A. 6 - Balsa wood and some commonly used foam core material systems. (Beckwith, 2008)

Core Material Family	Typical Density Range, kg/m³ (lb/ft³)	Shear Strength, MPa (psi)	Shear Modulus, MPa (ksi)	Compression Strength, MPa (psi)	Maximum Service Temperature, °C (°F)
Balsa Wood (closed end grain)	96-250 (6-16)	1.85-4.94 (270-720)	108-312 (15.7-45.3)	6.5-26.6 (945-3860)	165 (325)
Polyurethane Foam (PUR)	21-400 (1.5-25)	0.15-3.1 (20-450)	1.55-104 (0.23-15.0)	0.2-0.35 (29-50)	135 (275)
Polystyrene Foam (PS)	30-60 (2-4)	0.25-0.60 (36-90)	4.5-20 (0.65-2.9)	0.3-0.9 (44-130)	100 (212)
Polyvinylchloride Foam (PVC)	30-400 (2-25)	0.35-4.5 (50-655)	8.3-108 (1.2-15.7)	0.3-5.8 (44-840)	55-120 (130-250)
Polymethacrylimide Foam (PMI)	30-300 (2-20)	0.8-7.5 (115-1090)	19-290 (2.8-42.1)	0.8-16 (116-2325)	140 (285)
Polyetherimide Foam (PEI)	60-110 (4-7)	0.8-1.4 (120-200)	18-30 (2.6-4.4)	0.7-1.4 (100-200)	180-190 (355-375)
Styrene-acrylonitrile Copolymer Foam (SAN)	48-160 (3-10)	1.3-3.5 (180-510)	13.8-41.4 (2.0-6.0)	0.35-10.3 (50-1500)	135 (275)
Epoxy Foam	80-320 (5-20)	0.45-5.2 (65-755)		0.62-7.4 (90-1075)	177 (350)
Phenolic Foam	5-160 (0.5-10)	0.01-1.45 (1.4-210)		0.014-2.07 (2.0-300)	145-200 (300-390)
Carbon/Graphite Foams	30-560 (2-35)	0.05-3.9 (7.3-566)		0.2-60 (29-8700)	~2500 (~4530)

Table A. 7 - Comparison of core material relative costs and their characteristics and benefits. (Beckwith, 2008)

Core Material Family	Relative Core Material Cost	Characteristics and Benefits
Balsa Wood (closed end grain)	Low	Good shear strength, high fatigue endurance, easily bonded, easily finished, good temperature range, but absorbs moisture, potential for fungus
Polyurethane Foam (PUR)	Low	Good solvent resistance, good temperature capability, moderately fire resistant, wide density range of products
Polystyrene Foam (PS)	Low	Lowest temperature capability, lowest cost material, moderate mechanical properties, fairly fragile material
Polyvinylchloride Foam (PVC)	Low	High strength, high stiffness, easily bonded, good impact resistance, only moderate temperature capability
Polymethacrylimide Foam (PMI)	High	High dimensional stability at temperature, excellent mechanical properties, solvent resistance, low thermal conductivity, high strength and stiffness
Polyetherimide Foam (PEI)	High	Low moisture absorption, high thermal stability, high strength, good fire resistance, good dielectric properties
Styrene-acrylonitrile Copolymer Foam (SAN)	Moderate	No outgassing, high stiffness, high impact and fatigue strength, no environmental problems with resin or recycling
Epoxy Foam	Moderate	High strength and stiffness, compatible with numerous laminate systems, excellent high temperature properties, moderate fire resistance
Phenolic Foam	Moderate	Excellent fires/smoke/toxicity properties, somewhat brittle, good high temperature properties, very good insulator
Carbon/Graphite Foams	High	Excellent high temperature properties (best), high stiffness mechanical properties, high cost main deterrent, used as tooling materials as well as structures

Table A. 8 - Mechanical Properties of Honeycomb Materials - Typical Values at Room Temperature (Hexcel Composites, 2000)

PRODUCT CONSTRUCTION		COMPRESSION		PLATE SHEAR			
Density	Cell Size*	Stabilized		L Direction		W Direction	
kg/m ³ (lb/ft ³)	mm (in)	Strength MPa	Modulus MPa	Strength MPa	Modulus MPa	Strength MPa	Modulus MPa
3003 Aluminium							
29 (1.8)	19 (3/4)	0.9	165	0.65	110	0.4	55
37 (2.3)	9 (3/8)	1.4	240	0.8	190	0.45	90
42 (2.6)	13 (1/2)	1.5	275	0.9	220	0.5	100
54 (3.4)	6 (1/4)	2.5	540	1.4	260	0.85	130
59 (3.7)	9 (3/8)	2.6	630	1.45	280	0.9	140
83 (5.2)	6 (1/4)	4.6	1000	2.4	440	1.5	220
5052 Aluminium							
37 (2.3)	6 (1/4)	1.35	310	0.96	220	0.58	112
50 (3.1)	5 (3/16)	2.3	517	1.45	310	0.9	152
54 (3.4)	6 (1/4)	2.6	620	1.6	345	1.1	166
72 (4.5)	3 (1/8)	4.2	1034	2.3	483	1.5	214
83 (5.2)	6 (1/4)	5.2	1310	2.8	565	1.8	245
127 (7.9)	6 (1/4)	10.0	2345	4.8	896	2.9	364
130 (8.1)	3 (1/8)	11.0	2414	5.0	930	3.0	372
5056 Aluminium							
37 (2.3)	6 (1/4)	1.8	400	1.2	220	0.7	103
50 (3.1)	3 (1/8)	2.4	669	1.7	310	1.1	138
50 (3.1)	5 (3/16)	2.8	669	1.8	310	1	138
72 (4.5)	3 (1/8)	4.7	1275	3.0	483	1.7	193
HRH10 Nomex (Aramid)							
29 (1.8)	3 (1/8)	0.9	60	0.5	25	0.35	17.0
32 (2.0)	5 (3/16)	1.2	75	0.7	29	0.4	19.0
32 (2.0)	13 (1/2)	1.0	75	0.75	30	0.35	19.0
48 (3.0)	3 (1/8)	2.4	138	1.25	40	0.73	25.0
48 (3.0)	5 (3/16)	2.4	140	1.2	40	0.7	25.0
64 (4.0)	3 (1/8)	3.9	190	2.0	63	1.0	35.0
64 (4.0)	6 (1/4)	5.0	190	1.55	55	0.86	33.0
80 (5.0)	3 (1/8)	5.3	250	2.25	72	1.2	40.0
96 (6.0)	3 (1/8)	7.7	400	2.6	85	1.5	50.0
123 (7.9)	3 (1/8)	11.5	500	3.0	100	1.9	60.0
144 (9.0)	3 (1/8)	15.0	600	3.5	115	1.9	69.0
29 (1.8)	5 OX (3/16)	1.0	50	0.4	14	0.4	21.0
48 (3.0)	5 OX (3/16)	2.9	120	0.8	20	0.85	35.0
HRH78	Typical mechanical properties are similar to HRH10, however, the aramid sheet manufacturing tolerances are wider therefore minimum values may be reduced.						

Annex B - Numerical simulation results

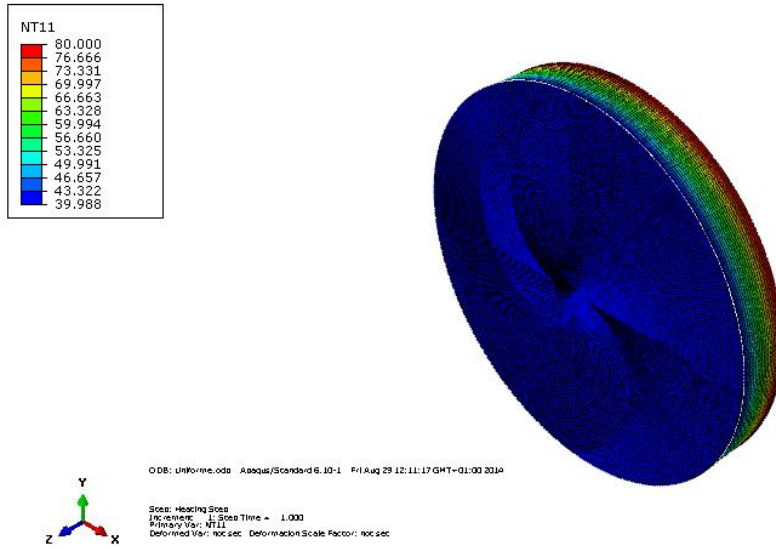


Figure B. 1 - Numerical results for the uniform model

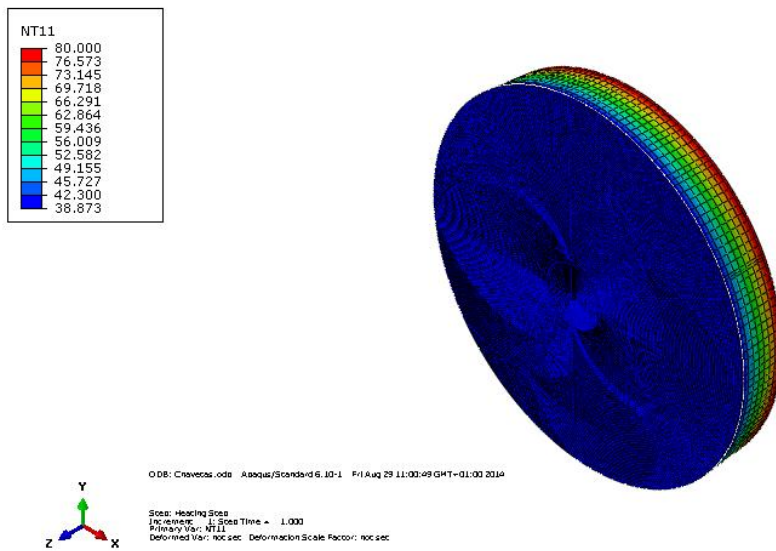


Figure B. 2 - Numerical results for the bracket model

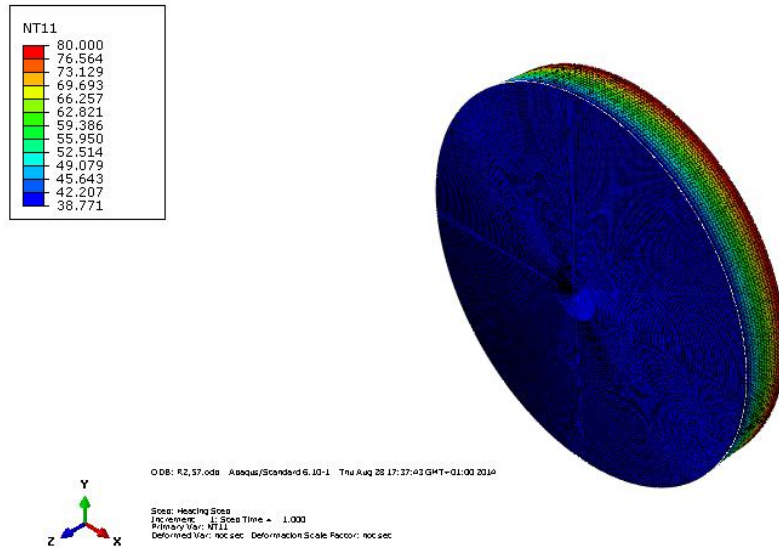


Figure B. 3 - Numerical results for the 5.14 mm circular hole model

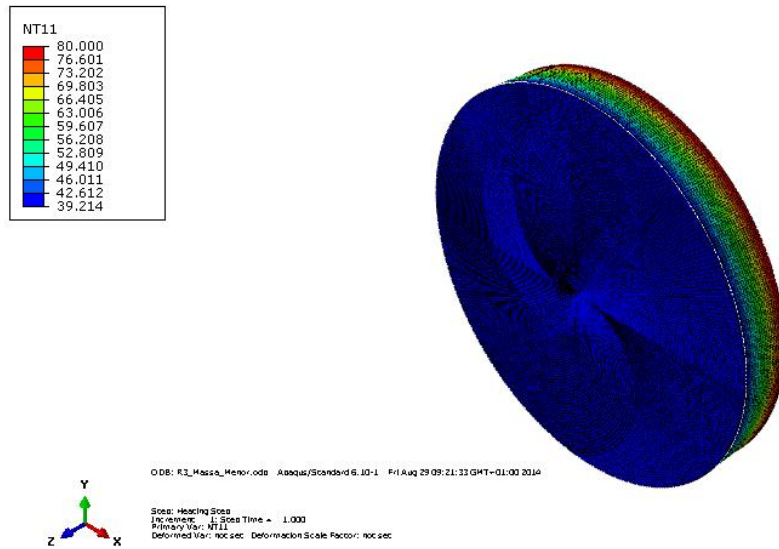


Figure B. 4 - Numerical results for the 6 mm circular hole (a) model (light version)

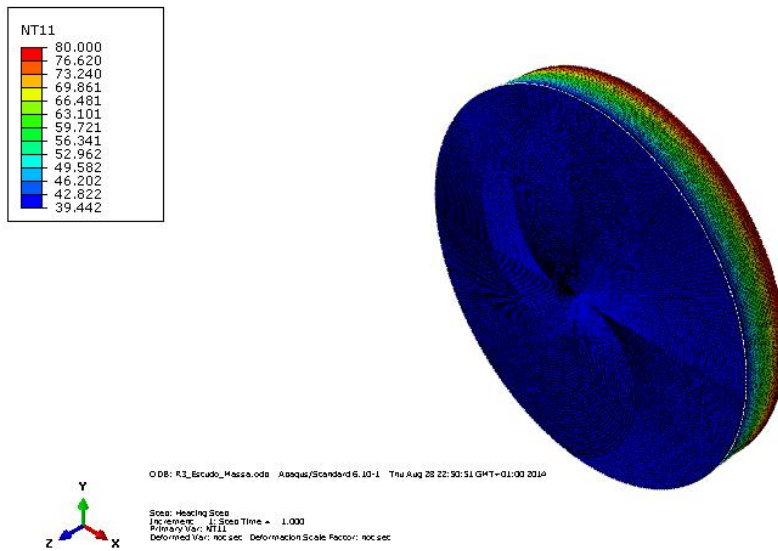


Figure B. 5 - Numerical results for the 6 mm circular hole (b) model (heavy version)

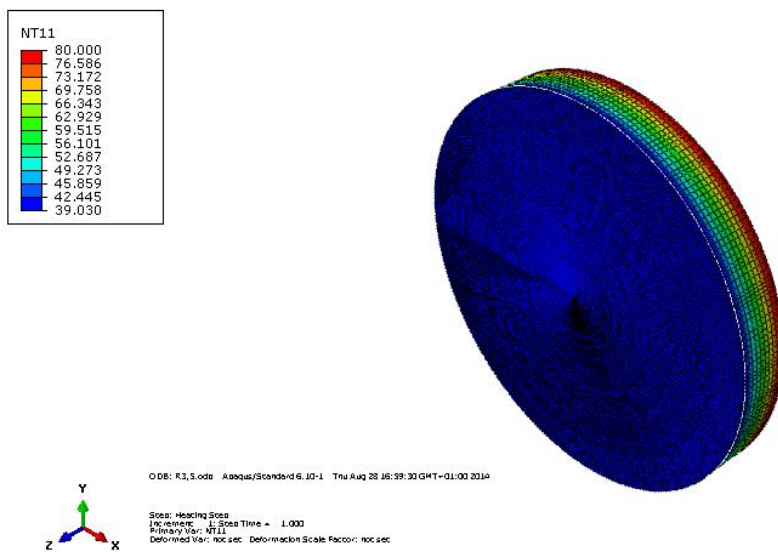


Figure B. 6 - Numerical results for the 7 mm circular hole model

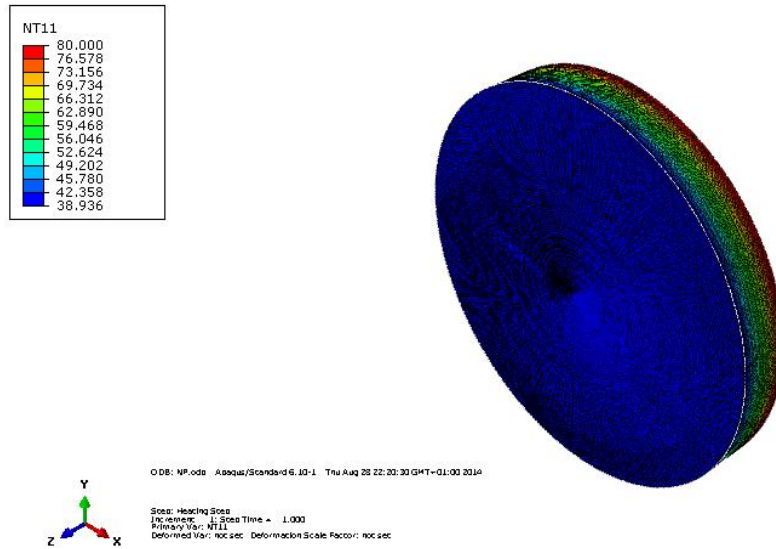


Figure B. 7 - Numerical results for the non through hole model without offset

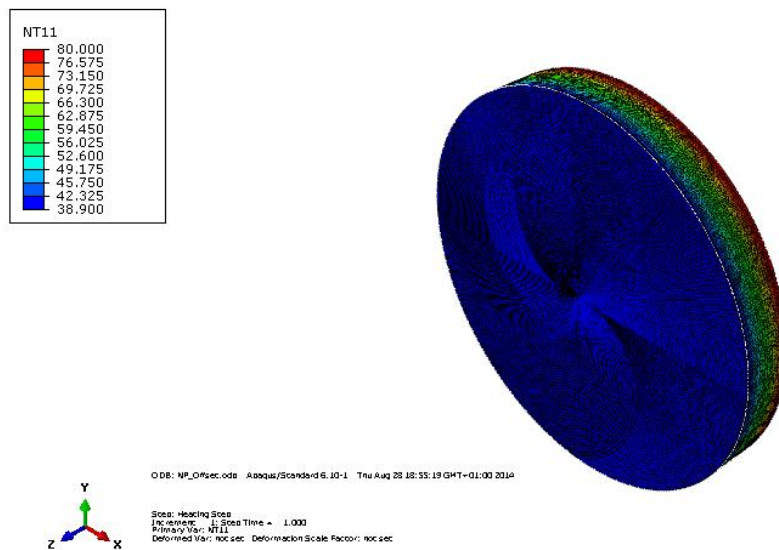


Figure B. 8 - Numerical results for the non through hole model with offset

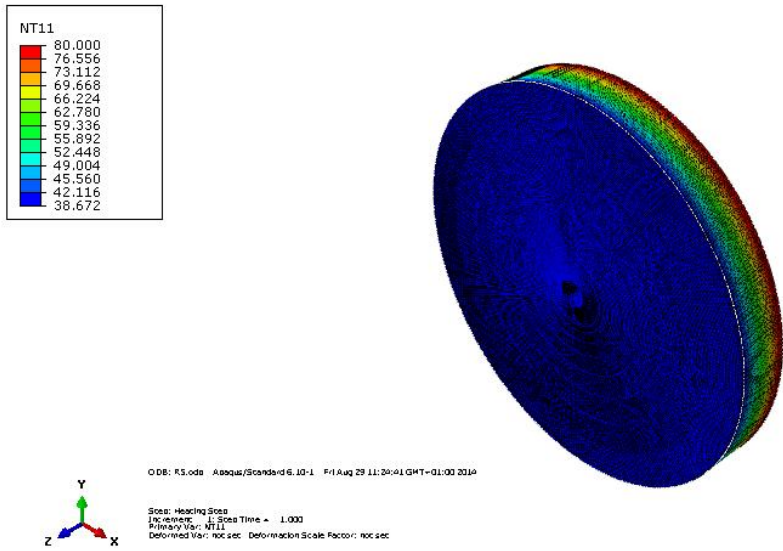


Figure B. 9 - Numerical results for the 10 mm circular hole model